

Developing the structure of rotating shaft in disc filter: ProTCorb Oy

Abstract

Author(s) Chau, Quan	Publication type Thesis, UAS	Completion year 2021
	Number of pages 68	
Title of the thesis Developing the structure of rotating shaft in disc filter: ProTCorb Oy		
Degree Mechanical Engineering and Technology Production		
Name, title and organisation of the thesis supervisor Tuomo Liimatainen, Senior Lecturer, LAB University of Applied Sciences		
Name, title and organisation of the client Esa Huttunen, ProTCorb Oy		
<p>Abstract</p> <p>The goal of the thesis is to strengthen and analyze the strength of latest model of Protcorb' s 26-disc-shaft, including static and fatigue in details. Moreover, the deflection is determined to avoid collisions during the operation. Subsequently, the structure of the shaft is developed in order to decrease the material usage and raise the inside cross-area of the inner channel.</p> <p>The static analysis is done by two methods, which are handled by MathCad and Finite Element Method by SolidWorks Simulation. In the analysis, the Von Mises stress and its safety factor are defined by both methods. Moreover, the deflection is determined by Simulation. The stress-based method is applied to define the fatigue lifetime and safety factor. Thus, The dimensions of the shaft are adjusted without changing the design to developing the structure .</p> <p>The result shown that there was not any failure and collision during the operation. After the structure is developed, the volume of the shaft without the channels decreased by 46%. The inside area of the updated channel increased by 71%, however, the material usage of the channel rose by 89%. Overall, the volume of entire updated shaft is 428708394.38 cubic millimeters which is an increase of 35%.</p>		
<p>Keywords</p> <p>Disc filter, rotating shaft, static analyzing, fatigue analyzing, developing the structure</p>		

Contents

1	List of abbreviations.....	4
2	Introduction.....	5
2.1	Background	5
2.2	Introduction of disc filter	5
2.2.1	Description	5
2.2.2	Filtration process	7
2.3	Goal of thesis.....	8
2.4	Delimitation.....	8
3	Theoretical research	9
3.1	Equilibrium.....	9
3.1.1	Equilibrium of the particle.....	9
3.1.2	Equilibrium of rigid body	9
3.1.3	Free body diagram (FBD)	10
3.2	Bending moment and shearing force in beam.....	10
3.2.1	Introduction.....	10
3.2.2	Shearing force and bending diagram	11
3.2.3	The flexure stresses.	13
3.3	Three-moment equation.....	15
3.4	Torsion	17
3.4.1	Torsional deformation of the circular shaft	17
3.4.2	Torsion formula.....	18
3.5	Von Mises stress equation.....	20
3.6	Definition and concepts of fatigue	21
3.6.1	Introduction.....	21
3.6.2	Cyclic loading	21
3.6.3	S-N curved	22
3.7	Stress-base method in fatigue analysing.	24
3.7.1	Notch effect	24
3.7.2	Modified Goodman equation.....	25
3.7.3	Factors affecting long-life fatigue strength.	26
3.7.4	Fatigue safety factor	28
3.8	Introduction of Finite Element Method (FEM).....	29
4	Static analyzation of rotating shaft	30
4.1	Features in strength analyzation	30
4.1.1	Bearing	30
4.1.2	Disc	31

4.1.3	The tubes	33
4.1.4	Gearbox.....	36
4.1.5	Water.....	39
4.2	4-disc-shaft.....	39
4.2.1	Handling method by Mathcad	39
4.2.2	FEM by SolidWorks Simulation.....	44
4.2.3	Conclusion.....	46
4.3	26-disc-shaft.....	46
4.3.1	Handling method	46
4.3.2	FEM by SolidWorks Simulation.....	50
4.4	Conclusion.....	51
5	Deflection.....	52
5.1	Introduction.....	52
5.2	Deflection of the 26-disc-shaft	52
6	Fatigue calculation.....	54
6.1	Introduction.....	54
6.2	Fatigue calculation.....	54
6.2.1	Mean stress.....	54
6.2.2	Amplitude stress	55
6.2.3	Notch factor	56
6.2.4	Reduction factor	56
6.2.5	Fatigue calculation.....	58
6.3	Conclusion.....	59
7	Developing the structure of the shaft.....	60
7.1	Introduction.....	60
7.2	Optimizing the usage of material.....	60
7.2.1	Decreasing the length of the drive end.....	60
7.2.2	Decreasing the thickness off the vat	61
7.3	Increasing the cross area of the inner channel.....	61
7.3.1	Introduction.....	61
7.3.2	Support plate	62
7.4	Inner channel.....	62
7.4.1	Strength analyzation of the updated shaft.....	62
7.5	Conclusion.....	64
8	Conclusion.....	65
9	Reference.....	66

Appendices

Appendix 1: The latest inner channel figures.

Appendix 2: The updated inner channel figures.

1 List of abbreviations

FEM as Finite Element Method

FBD as Free-Body-Diagram

kg as kilogram

kN as kilo Newton

m as meter

mm as milimeter

MPa as mega pascal

N as Newton

rpm as round per minute

W as Watt

2 Introduction

2.1 Background

In the present industrial revolution, new technologies such as cloud computing, machine learning, or Artificial Intelligence (AI) are applied in order to enhance the efficiency of production. There is a rule of thumb that the effectiveness of manufacturing and production process proportionately increases the amount of water consumption. In typical heavy industries, especially paper and pulp, water is used in every process, which accounts for 25000 gallons of water per ton of paper (Zero Gravity Filter). However, water is not an unlimited resource, hence, waste treatment takes an essential role in the production. There are several methods of water treatment, but the disc filter is the most ubiquitous method in the paper and pulp industry. In several companies, certain specific technology in the filtrate process is available, contributing to formation of critical competitive factor for the practitioner.

ProtCorb, a start-up in developing the structure and system of water treatment, has designed 3D models of their disc filter. In light of the shortcoming of such technology in practice, this thesis will put emphasis on the strength analysis and structure development..

2.2 Introduction of disc filter

2.2.1 Description

The disc filter is the device employed to filter the water in heavy industry such as paper milling. The device encompasses two main components, namely the rotating shaft and discs (Riker 1969).

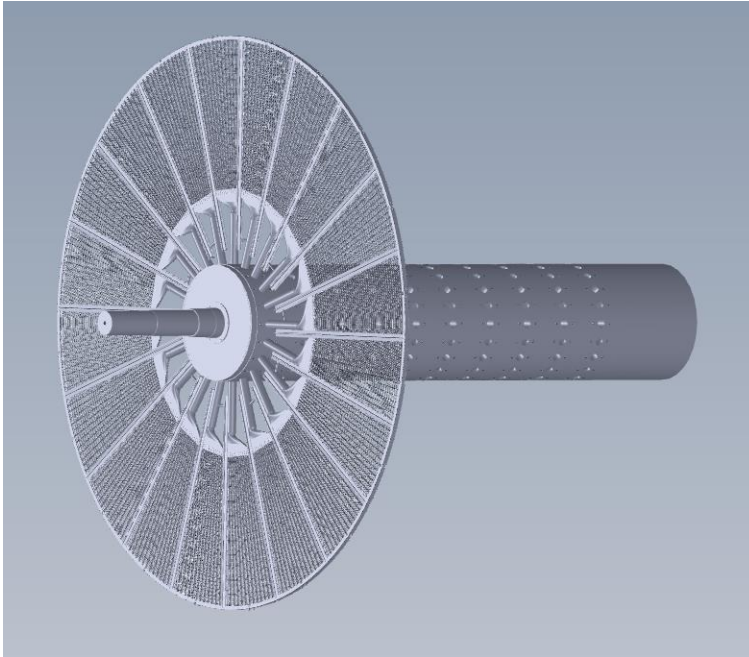


Figure 1. The 3D modelling of disc filter

The series of filter discs is assembled respectively through the vat. At one end of the vat, the drive-end shaft is assembled, and a trunnion valve is installed to control the filtration revolution which affects the rotation of the disc mounted on the shaft at the other end (Riker 1969).

Each of the filter discs is formed from several sectors which are staged independently on the vat. In turn, the sectors are connected with the control valve and each other by an inner channel, which is located inside the vat (Riker 1969).

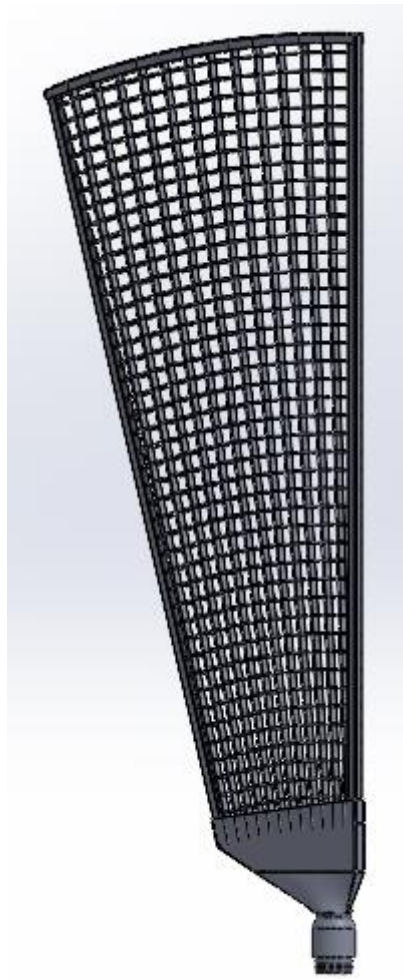


Figure 2. The sector of the shaft

The control valve is applied in a vacuum force from the barometric leg into the half of sectors which is drowned into unfiltered water during the cake (dust) forming phase. As a result, the filtration direction is inside out. (Riker 1969).

2.2.2 Filtration process

To begin with, the infiltrated water is pumped into the shaft from the valve side, enabling water to flow through 20 inner channels which are connected to the sectors, respectively. Because of the gravity and the vacuum force, the water flows through the sectors and is filtrated inside out. During the filtration, dust known as cake is formed on the haft downward of sectors as the shaft revolves. The sectors which are clanged by the cake are rotated upward, leaving the cake being removed by vacuum or water jet. Finally, removed cake is

conveyed from the filter media into the troughs, which are located between the discs or inside the vat.

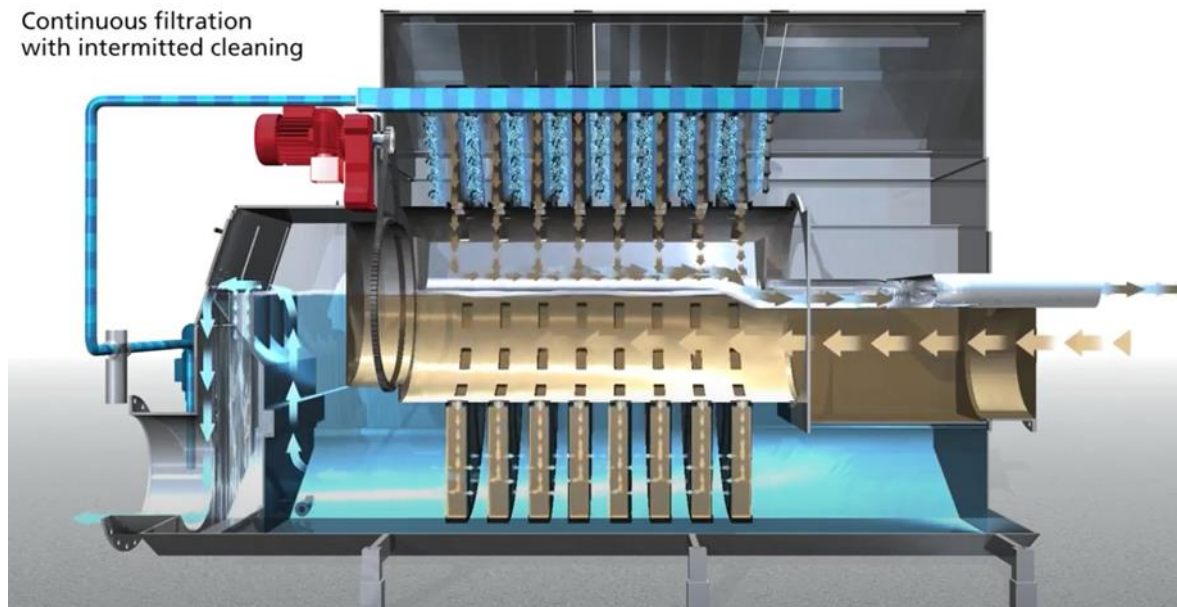


Figure 3. HUBER disc filter process (HUBERE SE 2017).

2.3 Goal of thesis

At the beginning of the thesis, the 3D models of the 26-disc-disc filter including the disc and shaft are designed. The static analysis by Simulation was done generally. There are 2 main tasks of the thesis, which one of those is strengthen analysis the latest model of shaft including static and fatigue in details. Moreover, the deflection is determined to avoid collisions during the operation. Subsequently, the structure of the shaft is developed in order to decrease the material usage and to raise the inside cross-area of the inner channel. Because the inner channel is the competitive factor between the companies, the figures of inner channel are hided from the reader by inserted in appendices.

2.4 Delimitation

There are two main parts in the filter disc, which are the shaft and disc. The thesis only studies in the shaft including vat, drive-end shaft, support plates and inner channels. The analysis includes static by Von mise stress and fatigue lifetime at the critical points. For decreasing the usage of the material, the dimensions are adjusted without changing the design of the shaft. However, in developing the area of the inner channel, the flow calculation and effect are neglected.

3 Theoretical research

3.1 Equilibrium

3.1.1 Equilibrium of the particle

The equilibrium known as static equilibrium is used for a particle when it is at rest or moving with a constant velocity, however, in most cases, the particle is at rest. The first Newton's law of motion is required to satisfy for keeping the equilibrium. The law which is shown in formula (1) said that the vector of resultant force applied on the particle is equal to 0 (Hibbeler 2004, 81).

$$\sum F = 0 \quad (1)$$

In addition, equilibrium also satisfies the second Newton's law which is written $\sum F = m * a$. Because the sum of force is equal to 0, $m*a$ equals 0, which leads to acceleration is equal to 0. Therefore, it is at rest or moves with constant velocity (Hibbeler 2004, 81).

3.1.2 Equilibrium of rigid body

The rigid body is applied by external forces and coupling moments, which are driven by gravity, contact forces, electricity and magnetism. Moreover, there are internal forces arising from the interaction between the particles and are dependent on Newton's third law. For information, the law illustrates that the internal force is equal but in the opposite direction, compared to the external force (Hibbeler 2004, 193).

On the basis of the upward heading method, the external forces and coupling moment can be combined into the resultant external force and coupling moment at any point on or off the body. As a consequence, the body is in equilibrium when the resultant external forces and coupling are equal to 0. The formulas (2) and (3) describe those (Hibbeler 2004, 194).

$$\sum F = 0 \quad (2)$$

$$\sum M = 0 \quad (3)$$

In order to apply the equilibrium equation, it is assumed that the body is rigid. Nevertheless, in reality, the body is deflected by the effects of loads. In most cases in engineering applications, the material of the body is steel or concrete with the deformation being really small. Hence, the body is assumed to be rigid and not deflect when the loads are applied. This

leads to the the direction of loads and their moment remaining fixed before and after the loads applied (Hibbeler 2004, 194).

3.1.3 Free body diagram (FBD)

So as to apply the equilibrium equations correctly, it is necessary to describe the known, unknown external forces and coupling moment; and internal forces as known as reactions. The free body diagram is an effective method to describe those forces. The free body diagram draws the shape of the body which becomes confined or "free" from other effects. It is essential to show the external forces and moments on the FBD when the equilibrium equations are applied. The FBD helps to understand the features of the body which is important in engineering solving (Hibbeler 2011, 143).

It is important to consider the support reactions in drawing the free body diagram. There are several types of reaction which exist at the points or supports of contact. They can be divided into two main types.

- The support avoids the translation of the body in the known direction by applying an internal force in the opposite direction.
- The support avoids the rotating of the body in the known direction by applying a coupling moment in the opposite direction (Hibbeler 2011, 143.).

3.2 Bending moment and shearing force in beam

3.2.1 Introduction

Beam is a long, slight structural member which is applied by loads penderdically to its longitudinal axis. These loads cause the deformation of the beam on the plane of these and the internal stress is generated to resist the loads (Hibbeler 2011, 503).

The design of the beam is determined by size, shape and material which are based on the bending and shearing stress and the deflection caused by the external loads.

The classification of the beam depends on the supporting condition. There are six types of supporting condition which are simply supported (two supports), continuos supported (two or more supports), cantilever (one support is fixed), overhang (two supports which at least one is not at the end), propped (two supports which one is fixed) and fixed (two fixed supports) (Onouye & Kane 2013, 333).

The actual connection conditions between beam and support are divided into 3 types which are roller, fixed and hinges (Onouye & Kane 2013, 334). In the fixed support, the translations

including vertical, horizontal and rotating are restricted. Furthermore, in roller support, the horizontal and rotating translations are allowed. In hinges support, there is a certain allowable rotation at the connection.

3.2.2 Shearing force and bending diagram

When any loads are applied to the beam, the beam must resist and remain the equilibrium. In order to remain in equilibrium, the internal force must exist to resist the external loads and moments. The stresses and deflection on the beam are dependent on the internal forces, load and moment, hence it is handy to “map” these into a diagram, indicating the detailed view of magnitude and direction of the forces and moment throughout the beam length. There are 2 main diagrams which are shearing force (V) and bending diagram. Figure 4 shown the load diagram, shearing force, and bending diagram, respectively (Onouye & Kane 2013, 337).

In order to formulate the diagrams, the origin and the positive direction of x need to be defined. In most cases, the origin is chosen on the left and the positive direction of x is on the right (Hibbeler 2011, 504).

In the diagrams, the slope of the shearing force and moment will be discontinuous at the points where the supports, loads, or moment are located. Therefore, it is important to divide the beam into the regions between any 2 discontinuous loads. For example, the x_1 , x_2 , and x_3 are the coordinates of the region AB, BC, and CD, respectively, which is shown in Figure 5 (Hibbeler 2011, 504).

It is vital to define the signed agreement of the “positive” and “negative” value of shearing force and moment. Although there are different conventions, the one that is often used in engineering practice is shown in Figure 6. The loading is positive when the direction of the distributed load is upward, the internal shearing force causes the moment in a clockwise direction and the moment causes the compression at the upward face of the beam (Hibbeler 2011, 504).

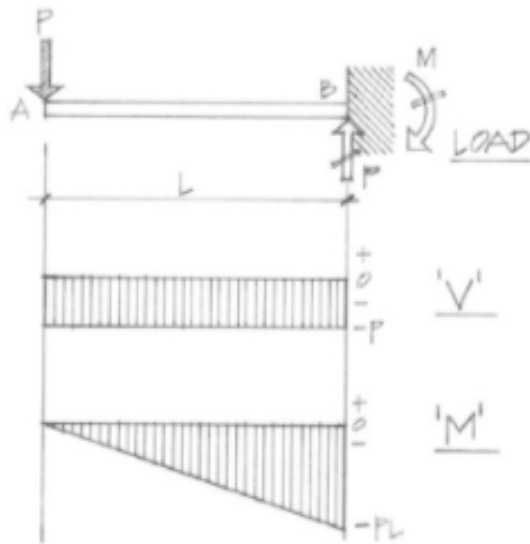


Figure 4. Load diagram, shearing force and bending diagram (Onouye & Kane 2013, 337)

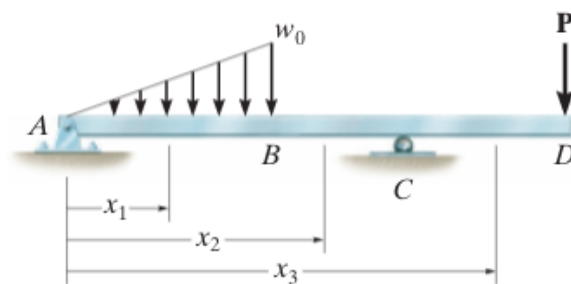


Figure 5. The example (Hibbeler 2011, 504).

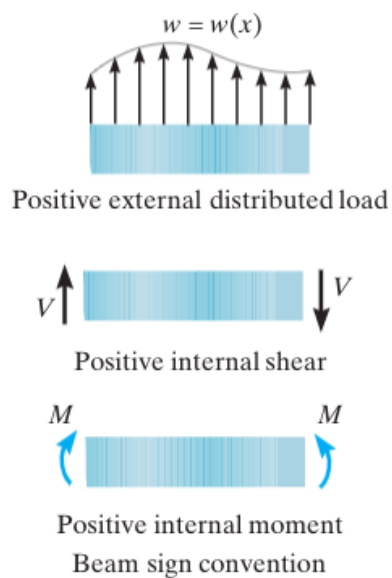


Figure 6. The positive sign of loading (Hibbeler 2011, 504).

3.2.3 The flexure stresses.

In order to calculate the bending stress, it is important to assume that the material behaves in a linear-elastic manner, hence Hooke's law is applied. The law gives the formula that $\sigma = E\epsilon$. A linear strain variation is the result of a linear stress variation, which is shown in Figure 7. In a normal variation of strain, the stress will fluctuate from 0 at the member's neutral axis to the maximum stress. It is indicated that 'c' is the farthest distance from the axis. By the feature of the triangle in the bending stress variation or the Hook's law, it is able to write the formula (4) (Hibbeler 2011, 531) .

$$\sigma = -\left(\frac{y}{c}\right) * \sigma_{max} \quad (4)$$

Equation (4) presents the distribution of stress over the cross-section area. It is critical to convert the sign of the formula. The moment which acts in the positive x-direction is positive, and the stress value is positive when the y value is the opposite sign. The condition in which the resultant force caused by the distributed stress over the cross area is zero, needs to be satisfied. The bending stress variation of Figure 7 shows that the force dF which is equal $\sigma * dA$ applies to the arbitrary element. Hence, formula (5) is required and developed to formula (7) (Hibbeler 2011, 531-532).

$$F_R = \sum F_x \quad (5)$$

$$\leftrightarrow 0 = \int_A dF = \int_A \sigma * dA = \int_A -\left(\frac{y}{c}\right) * \sigma_{max} * dA = -\frac{\sigma_{max}}{c} * \int_A y * dA \quad (6)$$

$$\leftrightarrow 0 = \int_A y * dA \left(\frac{\sigma_{max}}{c} \neq 0\right) \quad (7)$$

Where:

F_R : The resultant force

F_x : The force in x direction which is describe in bending stress variation of Figure 7

From equation (7). it can be said that the first moment of the cross-section area must be zero at the axis. The condition is only satisfied when the neutral axis and the horizontal centroid axis are duplicated. When the centroid is defined, the neutral axis of the cross area is determined (Hibbeler 2011, 532).

The requirement that the resultant internal moment and the moment caused by the distributed stress about the neutral axis are equal can be used to determine the bending stress.

In Figure 7, the moment of dF which is dM about the axis is equal $y * dF$. Because $dF = \sigma * dA$ and formula (7), the formula (8) for the entire area are formed (Hibbeler 2011, 504).

$$(M_R)_Z = \sum M_z \quad (8)$$

$$M = \int_A y * dF = \int_A y * (\sigma * dA) = \int_A y * \left(\frac{y}{c}\right) * \sigma_{max} * dA \quad (9)$$

$$\leftrightarrow M = \frac{\sigma_{max}}{c} * \int_A y^2 * dA \quad (10)$$

The integral in the equation is called the moment of inertia, the cross-section area. The moment of inertia of the cross section which is symbolized as I computed about the neutral axis. Therefore, the formula to calculate the maximum bending stress is written as formula (11) (Hibbeler 2011, 532-533).

$$\sigma_{max} = \frac{M * c}{I} \quad (11)$$

where:

σ_{max} : The maximum bending moment which occurs at the farthest point from the axis

M : The internal ending moment

I : The moment of inertia of the cross-section area

c : The farthest distance from the axis

Because $\sigma_{max}/c = -\sigma/y$, the bending moment at the point which the distance from the axis is y , is calculated by the formula (12).

$$\sigma = -\frac{M * y}{I} \quad (12)$$

In case the cross-section of the shaft is a solid circle, the moment of inertia I can be defined by the formula (13) (Hibbeler 2011, 533).

$$I = -\frac{\pi * d^4}{64} \quad (13)$$

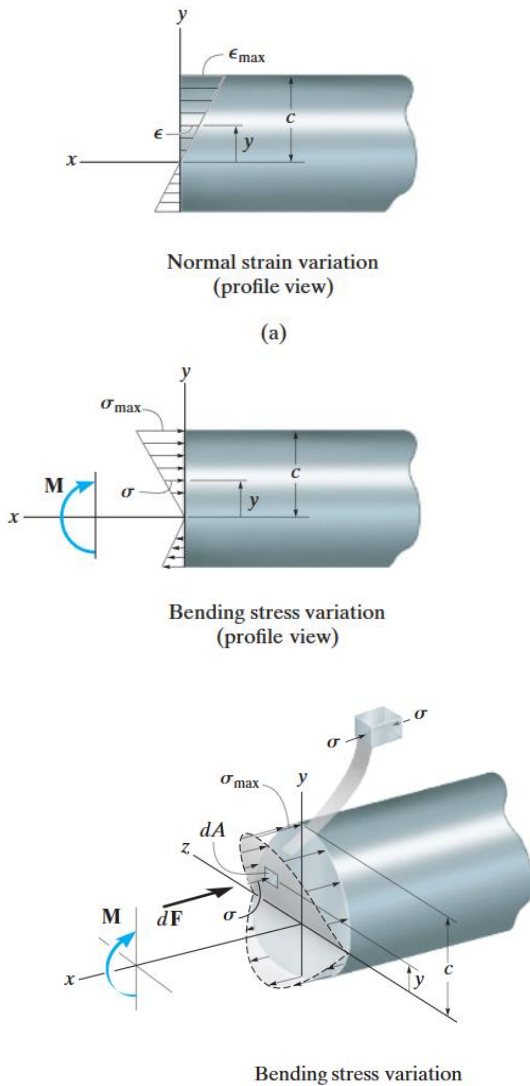


Figure 7. (Hibbeler 2018, 531).

3.3 Three-moment equation

The three-moment equation can be applied in any 2 spans (regions) of a continuous beam. For n number of regions, $(n-1)$ equations can be formulated which satisfy the equilibrium condition of a rigid body (eGyanKosh 2017, 27).

Let AB and BC are 2 spans of continuous beam ABC, which is shown in Figure 8a. The length of AB and BC are L_1 and L_2 , in turn. The moment of inertia of AB and BC are I_1 and I_2 , respectively (eGyanKosh 2017, 27).

The bending diagram which is caused by the external loads is shown in Figure 8b. Below, the diagram is the bending moment of unknown moments at the supports which are M_A , M_B and M_C . The upper diagram shows the bending moment diagram of the region AB

and BC separately, which are the simple support conditions (2 supports). Assuming A_1 and A_2 are the areas of the bending diagram subjected by the external loads of span AB and BC, in turn. x_1 and x_2 is the distance between 2 ends to the gravity center of the regions. The slopes at B in Figure 8c which is the deformation plot of the beam are the same on the left and right sides (eGyanKosh 2017, 28).

$$\theta_{BA} = \theta_{BC} \quad (14)$$

Because the angle is small, the slopes approximate the formula (14), which t_{BA} and t_{BC} are the vertical deviation with respect to the tangent at B of A and C, respectively (eGyanKosh 2017, 28).

$$\theta_{BA} = \frac{t_{BA}}{L_1}; \quad \theta_{BC} = \frac{t_{BC}}{L_2} \quad (15)$$

$$\frac{t_{BA}}{L_1} = -\frac{t_{BC}}{L_2} \quad (\text{opposite direction in Figure 8c}) \quad (16)$$

The deviation of A which can be defined by moment area method, is moment of $\frac{M}{EI}$ area between A and B about A in Figure 8c (eGyanKosh 2017, 28).

$$t_{AB} = \sum \left[\text{Area of } \frac{M}{EI} \text{ diagram between A and B} * x_1 \right]$$

$$= \frac{1}{E_1 * I_1} * (A_1 * x_1 + \frac{L_1 * M_A}{2} * \frac{L_1}{3} + \frac{L_1 * M_B}{2} * \frac{2L_1}{3}) \quad (17)$$

$$t_{BC} = \frac{1}{E_2 * I_2} * (A_2 * x_2 + \frac{L_2 * M_B}{2} * \frac{L_2}{3} + \frac{L_2 * M_C}{2} * \frac{2L_2}{3}) \quad (18)$$

The combination of formula (15), (16) and (17) develop the three-moment equation (eGyanKosh 2017, 28).

$$\frac{M_A * L_1}{E_1 * I_1} + 2 * M_B * \left(\frac{L_1}{E_1 * I_1} + \frac{L_2}{E_2 * I_2} \right) + \frac{M_C * L_2}{E_2 * I_2} = \frac{-6 * A_1 * x_1}{E_1 * I_1 * L_1} + \frac{-6 * A_2 * x_2}{E_2 * I_2 * L_2} \quad (19)$$

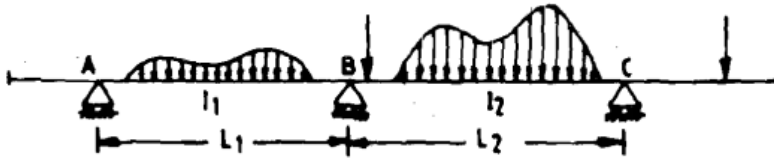


Figure 8a. (eGyanKosh 2017, 28)

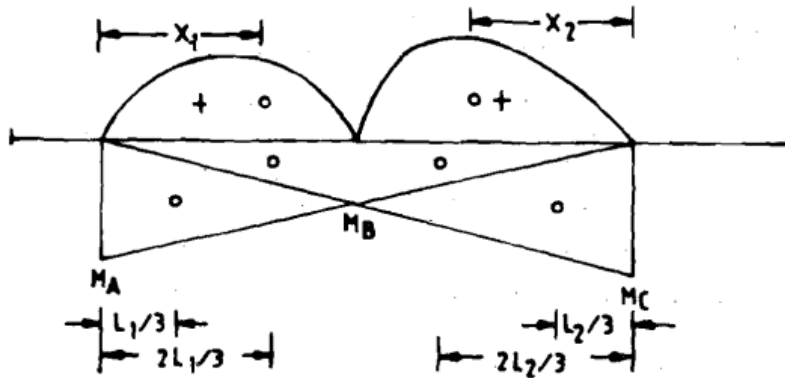


Figure 8b. (eGyanKosh 2017, 28)

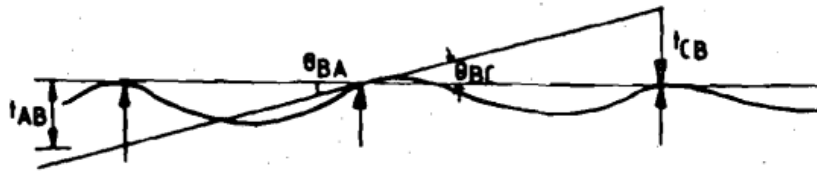


Figure 8c. (eGyanKosh 2017, 28)

3.4 Torsion

3.4.1 Torsional deformation of the circular shaft

Torque is a moment, which twists the member about its longitudinal axis. The torque is a critical effect in rotating structures such as drive end, shaft used in machinery or vehicles. Therefore, it is crucial to determine the stress and deformation on the shaft when the torque load is applying. The physical illustration when the torque is applied to the circular shaft can be seen by considering the material of the shaft is rubber, which is highly deformable. When the torque is applied, the cross-section area and the longitudinal grid lines which are marked on the shaft distort into the pattern. When the shaft is twisting, the circle remains its own shape, and the longitudinal grid line becomes a helix which intersects the circle at an equal angle. The cross-section face at the end of the shaft remains flat which means that they do not warp or bulge in or out. As a result, if the angle of rotation is small, it is assumed that the length and the radius of the shaft are unchanged. Figure 9 shows the illustration of the shaft before and after the torque applies (Russell 2018, 453) .

If the shaft is fixed on one end and there is a torque applied at the other end, the form of the shaft is shown in Figure 9. A radial line, which belongs to a cross-section face at a distance x from the fixed end will rotate through an angle $\phi(x)$. The angle $\phi(x)$ is called the twist angle (Hibbeler 2018, 454).

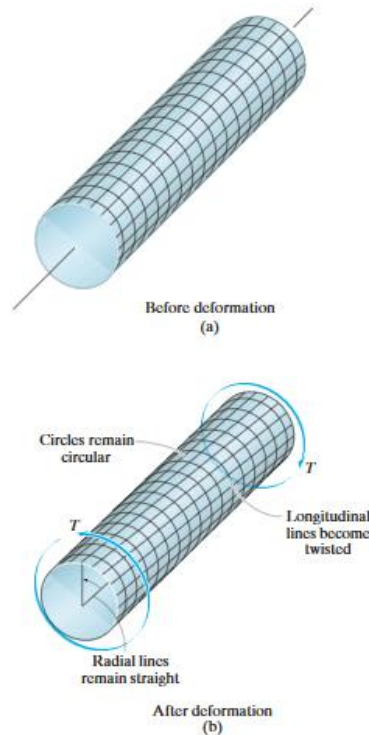


Figure 9. The shaft before and after the torque applies (Hibbeler 2018, 453) .

3.4.2 Torsion formula

When an external torque is placed into the shaft, an internal torque, which is equal and opposite to the external one, is produced inside the shaft. Hook's law is applied which is $\tau = G * \gamma$, in case the material is linear elastic. Therefore, a linear variation of shear stress is the result of a linear shear strain variation along any radial line on the cross-section face. The torque fluctuates from 0 at the longitudinal axis to the maximum value, in the shear-strain variation. The Figure shown the variation on a front face of a selected number of the element. The variation located at the transitional radial ρ and at the outer radius c . Taking advantage of the feature of the triangle or Hook's law, formula (20) is written (Hibbeler 2018, 45).

$$\tau = \frac{\rho}{c} * \tau_{max} \quad (20)$$

The equation represents the shear-stress distribution, in which radial position ρ is the element. It determines the distribution of stress over the cross-section area of the shaft. In

order to apply the formula, the torque generated by the stress distribution over the entire area must be equal to the resultant internal torque at the section. Each element of the area dA which is located at ρ in Figure 10 is controlled by a force of $dF = \tau * dA$. And the equation of the torque caused by this force is $dT = \rho * (\tau * dA)$. From that, the equation of the entire area is structured as formula (21) (Hibbeler 2018, 457).

$$T = \int_A \rho * (\tau * dA) = \int_A \rho * \frac{\rho}{c} * \frac{\tau_{max}}{dA} = \frac{\tau_{max}}{c} \int_A \rho^2 * dA \quad (21)$$

The integral in the equation depends only on the geometry of the shaft. It computes the longitudinal axis, which represents the polar moment of inertia of the shaft cross-section area. The integral, which is symbolized as J , rewritten in the formula (22) (Hibbeler 2018, 457)

$$\tau_{max} = \frac{T * c}{J} \quad (22)$$

where:

τ_{max} : The maximum torsion stress in the shaft

T : The resultant torque moment at the cross-section

c : The outer radius of the shaft

J : The polar moment of inertia

The combination between 2 equations (20) and (22) is able to determine the torque stress at the intermediate distance ρ .

$$\tau = \frac{T * \rho}{J} \quad (23)$$

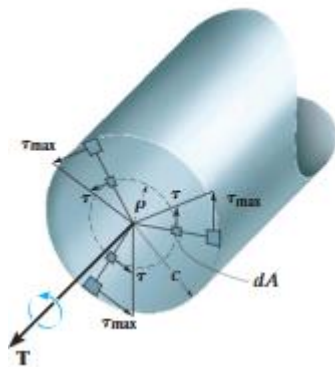


Figure 10. Torque stress varies linearly along each radial line of the cross-section (Hibbeler 2018, 456) .

In case the cross-section of the shaft is a solid circle, the polar moment inertia J can be defined by a form of a differential ring or annulus which uses an area element and shown in Figure 11. Thus, the formula has a thickness $d\rho$ and the circumference $2\pi\rho$.

$$dA = 2\pi * d\rho * \rho \text{ (for the ring)} \quad (24)$$

$$J = \int_A \rho^2 * dA = \int_0^c \rho^2 * (2\pi * \rho * d\rho) = 2\pi \int_0^c \rho^3 * d\rho = \frac{\pi}{2} * c^4 \quad (25)$$

The polar moment of inertia is positive, and its common unit is mm^4 (Hibbeler 2018, 458)

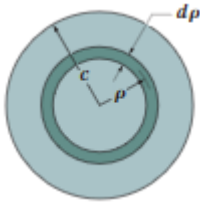


Figure 11. (Hibbeler 2018, 458)

3.5 Von Mises stress equation

Von Mises criterion is commonly used for designing ductile material engineering components. It evaluates the design under the limit and works in a safe manner. The Von Mises stress is developed from distortion energy to decide if the ductile material is failed under the subjected loadings. The member will fail when the Von Mises stress is greater than the allowable yielding strength of the material. Most of transmission shafts can be analyzed with the form of Von Mises equation in formula (26)

$$\sigma_v = \sqrt{((\sigma_b + \sigma_t))^2 + 3 * (\tau + \sigma_s)^2} \quad (26)$$

where:

σ_b : The bending stress

σ_t : The tensile stress

τ : The torque shear stress

σ_s : The direct shear stress

The safety factor of the engineering component is calculated by the formula

$$n = \frac{R_E}{\sigma_v} \quad (27)$$

where:

R_E : The yielding strength of the material

3.6 Definition and concepts of fatigue

3.6.1 Introduction

The components such as the drive shaft in the machinery, vehicle, and structures are applied frequently by repeated loads and the resultant of the cyclic load, which may cause microscopic physical damage to the materials (Dowling 1999, 357).

Even the maximum resultant stress on the structure is lower than the given material's ultimate strength, the damage may continuously grow until it turns into the crack or the other macroscopic damage which leads to the failure of the structure. The process of failure and damage caused by the cyclic loadings is called 'fatigue'. This term appears in an early investigator, which the cyclic stresses produce a gradual, not readily detectable, changes in the strength of the material (Dowling 1999, 357).

There are three main approaches to analyze and design against fatigue failure. The traditional method, which is a stress-based approach, was developed to fundamental its present form by 1955. This method revolves around the nominal (average) stresses in the affected region of the component are applied, is applicable in most engineering cases. The nominal stress amplitude which can be resisted under the cyclic loading, is defined by the mean stress and include the raising effects such as groove, holes, keyways, and fillet. The strain-based method analyses detailly in localized yielding which may occur at stress raiser during the cycling loading. The last approach applied the fracture mechanics method to treat special growing crack (Dowling 1999, 358).

3.6.2 Cyclic loading

In the practical application, there is not pure static loading, which is not constant. The loading is assumed static when it has a small or extremely low variation. In most engineering cases, the maximum and minimum stress levels are constant. It is called constant amplitude stressing which is shown in Figure 12 (Dowling 1999, 359).

The stress range, which is the difference between the maximum and minimum stresses value, is defined by $\Delta\sigma = \sigma_{max} - \sigma_{min}$. The mean stress which is symbolized by σ_{mean} is the average between the maximum and minimum ones. The stress amplitude which is σ_a , is half of the stress range. The mathematic formulas (28) (29) and (30) suppress the definitions (Dowling 1999, 359).

$$\sigma_a = \frac{\Delta\sigma}{2} = \frac{\sigma_{max} - \sigma_{min}}{2} \quad (28)$$

$$\sigma_m = \frac{\sigma_{max} + \sigma_{min}}{2} \quad (29)$$

$$\sigma_{max} = \sigma_m + \sigma_a; \quad \sigma_{min} = \sigma_m - \sigma_a \quad (30)$$

The values of range and amplitude stresses are always positive because the maximum is bigger than the minimum stress. In quantities, the maximum, minimum, and mean stresses can be positive or negative. The ratios which are symbolized as R are A, are the stress ratio and amplitude ratio, in turn. The relationship between these variables are shown as formulas (Dowling 1999, 360).

$$R = \frac{\sigma_{min}}{\sigma_{max}}; \quad A = \frac{\sigma_a}{\sigma_m} \quad (31)$$

$$\sigma_a = \frac{\Delta\sigma}{2} = \frac{\sigma_{max}}{2} * (1 - R); \quad \sigma_m = \frac{\sigma_{max}}{2} * (1 + R) \quad (32)$$

$$R = \frac{1 - A}{1 + A}; \quad A = \frac{1 - R}{1 + R} \quad (33)$$

The cyclic system is also applied in the other variables such as force, strain, bending moment, and normal stress.

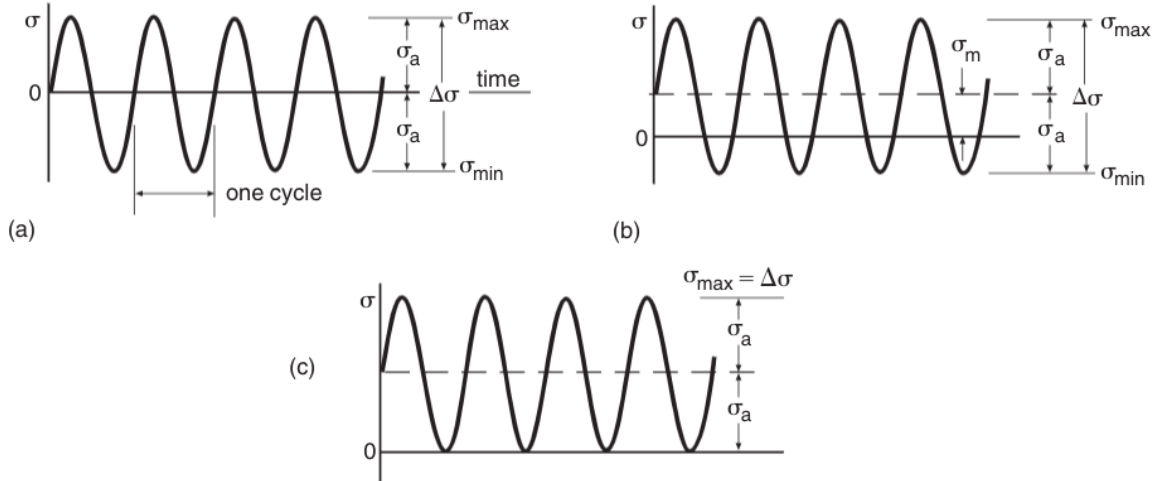


Figure 12. 3 types of cyclic loading (Dowling 1999, 360).

3.6.3 S-N curved

In case a test specimen of the material is applied by cyclic stress, a fatigue crack or damage will be developed. If the test gives out a higher stress level, the number of cycles to failure which is fatigue life will be smaller. The results of tests which at least 3 specimens, from a

number of stress level may be plotted to a stress-life curve as known as S-N curve (Dowling 1999, 363).

The amplitude or mean stress is commonly plotted versus the fatigue life to failure N_f which is shown in Figure 13 . (Dowling 1999, 363).

The number of cycles to failure changes rapidly with stress level, hence, the fatigue life is plotted on a logarithmic scale or sometimes double logarithmic scale. Therefore, it is difficult to plot the cycle of life on a linear scale, which is shown in Figure 13 .In the figure, the same data are plotted on logarithmic and linear scale. On the linear plot which is the right plot, the fatigue life cannot be read accurately (Dowling 1999, 363).

The equations (34), (35) present the mathematical representation of the curved in logarithmic and approximately linear scale, respectively (Dowling 1999, 363-364).

$$\sigma_a = C + D * \log N_f \quad (34)$$

$$\sigma_a = A * N_f^b \quad (35)$$

where:

C: The constant describes intersection to y-axis

D: The constant describes the slope of curve

A: The slope of approximately linear equation

b: The constant

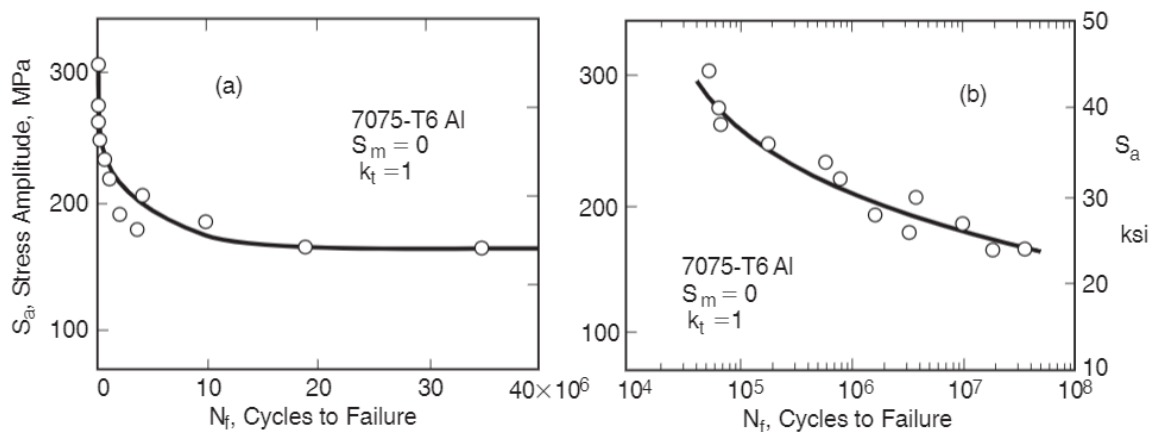


Figure 13.S-N curve from the test of rotating bending and unnotched specimen (Dowling 1999, 363).

3.7 Stress-base method in fatigue analysing.

3.7.1 Notch effect

In mechanical designing, the geometric discontinuities including fillet, groove, keyway, and hole, are hard to avoid. Therefore, the stress is locally raised, which is called stress raiser. The stress raiser, which is generalized and known as notches, decreases the resistance of the component to fatigue failure (Dowling 1999, 420).

The elastic stress concentration factor, which is symbolized as k_t , is used to define the harshness of the notch. Moreover, the factor is the ratio of the local notch stress to the nominal stress. Besides elastic stress concentration factor, there are also additional factors that need to be considered in fatigue analysis (Dowling 1999, 421).

The most effective method to analyse the notch factor is the notch sensitivity q and the common formulas, which are developed by H. Neuber to calculate the notch sensitivity, and the fatigue notch factor, are shown in formulas (36a), (36b) and (37), respectively (Dowling 1999, 426-429).

$$q = \frac{k_f - 1}{k_t - 1} \quad (36a)$$

$$q = \frac{1}{1 + \sqrt{\frac{\beta}{\rho}}} \quad (36b)$$

$$k_f = 1 - q * (k_t - 1) \quad (37)$$

where:

β : The material Neuber's constant which is defined by the graph in Figure 13

ρ : The notch radius

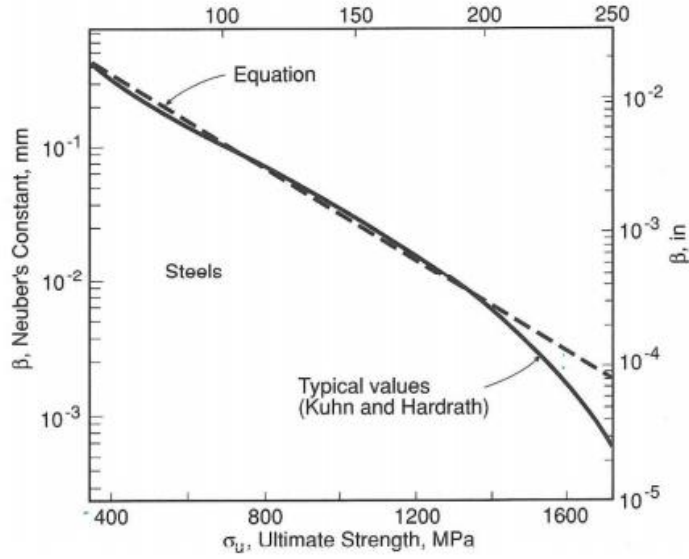


Figure 14. Neuber's material is constant for steel as a function of ultimate strength. (Dowling 1999, 427).

The formula (38) shown that the notch factors are affect to the Von Mises equation

$$e_{vm} = \sqrt{(k_{fb} * \sigma_b + k_{ft} * \sigma_t)^2 + 3 * (\sigma_s^2 + (k_{f\tau} * \tau)^2)} \quad (38)$$

where:

$k_{fb}, k_{ft}, k_{f\tau}$: The fatigue notch factor of bending, tensile and torsion stress, respectively

$\sigma_b, \sigma_t, \sigma_s, \tau$: The bending, tensile, direct shearing and torsion stress.

3.7.2 Modified Goodman equation

Depending on the normalized amplitude-mean diagram and stress-life curve for axial loading of the particular case, the equation which is shown in formula (39), is developed from Goodman's proposal by Smith in 1942. They are called modified Goodman equation (Dowling 1999, 391).

$$\frac{\sigma_e}{\sigma_{er}} + \frac{\sigma_m}{\sigma_u} = 1 \quad (39)$$

where:

σ_e : The fatigue limit of any mean stress

σ_{er} : The fatigue limit for zero mean stress

σ_m : The mean stress

σ_u : The ultimate strength

There are different fatigue limits in different material. Therefore, it is convenient to consider the ratio of fatigue limit to the ultimate strength, which is symbolized as m_e (Dowling 1999, 441).

$$m_e = \frac{\sigma_{er}}{\sigma_u} \quad (40)$$

For low and intermediate strength steel, regarding the common application, the value of the ratio is 0.5. Hence, the combination of formula (39) and (40) give the formula (41) which calculate the fatigue limit for the material with a yielding strength less than 1400 MPa.

$$\sigma_e = \frac{1}{2} * (\sigma_u - \sigma_m) \quad (41)$$

3.7.3 Factors affecting long-life fatigue strength.

Besides the notch factor which reduces the fatigue strength, there is a number of factors that affect the long-life fatigue strength which is often reduced.

The larger the size member in bending or torsion is, the more the fatigue strength decreases. Because the growth of stress with depth is less sudden in larger cross-section, the size factor which is symbolized as m_d , affects significantly to the fatigue strength. The size factors are defined in Table 1 which was developed by Dowling or by the formula of Niemann and Winter which is shown in formula (42). (Dowling 1999, 446; Niemann et al. 2005, 102).

Size (stress gradient) factor: m_d	Bending or torsion ²	
	$d < 10$ mm	1.0
	$d = 10$ to 50 mm	0.9
	$d = 50$ to 100 mm	0.8
	$d = 100$ to 150 mm	0.7
	Axial	0.7 to 0.9 ³

Table 1. Size factor by Dowling (Dowling 1999, 446).

$$m_d = \frac{1 - 0.7686 * a_d * \log\left(\frac{d}{7.5mm}\right)}{1 - 0.7686 * a_d * \log\left(\frac{d_{Ref}}{7.5mm}\right)} \quad (42)$$

Depending on the cross section and the material of the member, variables are defined by the Table 2 and 3.





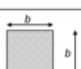
Cross-section shape	d_{eff}	
	Hardened steels, cast materials GJS, GJMB, GJMW, GJM	Non-alloyed construction steels, general cast iron
	d	d
	$2s$	s
	$2s$	s
	$\frac{2b-s}{b+s}$	s
	b	b

Table 2 (Niemann et al. 2005, 102)

Material type	d_{ref} (mm)	a_d
Non-alloyed construction steel	40	0,15
QT steels (EN 10831-1) hardened	16	0,3
QT steels (EN 10831-1 & 2) normalised	16	0,1
Large diameter QT steels (SEW 550) hardened	250	0,2
Large diameter QT steels (SEW 550) normalised	250	0
Cast iron GJS (EN 1563)	60	0,15
General steel cast (EN 1681)	100	0,15

Table 3. 2 (Niemann et al. 2005, 103)

In addition, the surface finish factor which is symbolized as m_s affects meaningfully to the fatigue strength. If the finished surface is rougher than the polished one of a typical smooth test specimen, the fatigue strength decreases. The fatigue limit reduces by around 10% when the surface is ground carefully. There are a number of typical surface conditions and the graph in Figure 15 illustrating the relation between those and surface factors.

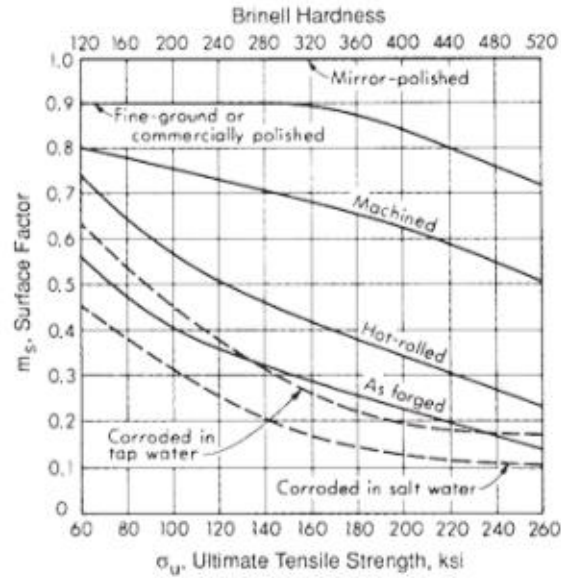


Figure 15. The effect of different surface finish on the fatigue limit of steel (Niemann et al. 2005, 105).

There are various factors that affect the fatigue strength such as temperature, microstructure layer, corrosive environment. The factors can be negative or positive and depend on each engineering application, the factors are researched. These other factors are symbolized as m_0 (Dowling 1999, 444).

The combination of factors is defined by multiplying all of them which affect the application. It modifies the fatigue limit σ_{erb} to the lower one σ_{er} (Dowling 1999, 444).

$$m = m_d * m_s * m_0 \quad (43)$$

$$\sigma_{em} = m * \sigma_e \quad (44)$$

3.7.4 Fatigue safety factor

The fatigue safety factor is defined by the formula.

$$s = \frac{\sigma_{em}}{\sigma_a} \quad (45)$$

Where:

σ_{em} : The modified fatigue limit.

σ_a : The amplitude stress.

3.8 Introduction of Finite Element Method (FEM)

Finite Element Method, as known as FEM, is a computerized mathematical technique for collecting approximate analytical solutions to the abstract equations to forecast the physical response of members which is subjected to external loadings (Burnett 1987, 3).

The FEM can be applied in many fields of engineering and mathematical problem which are solid mechanics, heat transfer, fluid mechanics electromagnetism, and acoustic. The method is useful in solving complicated models filled with unusual geometry or different materials (Burnett 1987, 3-4).

In Finite Element Analysing (FEA), there are several concepts that the method will analyse, including system, domain, governing equation, and loading condition (Burnett 1987, 5).

The system is a physical object, which is composed of one or more several types of material such as solid, gases, plasma, liquid.

The domain is the region of space, which is obtained by the system. The domain is divided into smaller, simple parts which are called finite elements. The elements connect with each other without gaps and overlapping. The element is obtained by points which is called node, and the collection of the element is called mesh (Burnett 1987, 5).

The governing equations describe a relation or balance of physical property such as mass, energy or momentum by differential equations. Besides, it can be an integral equation that expresses variational principle. The typical material behaviour and physical property are described by the constitutive equation (Burnett 1987, 5).

Loading conditions are the external loads or properties, which affect the system such as forces, temperature, current (Burnett 1987, 5).

First of all, the governing equation of each element, which is called the element equation is defined and solved. A linear combination of low-order polynomials which is called shape function approximates the solution of the element equation. Second, The element equations are made suitable at a common node which 2 or more elements share which are called continuity conditions. Then, the global stiffness and mass matrices are developed which form a lumped parameter discrete model of the structure. Lastly, a numerical displacement solution is collected (Burnett 1987, 8-11).

4 Static analyzation of rotating shaft

4.1 Features in strength analyzation

4.1.1 Bearing

The rotating shaft is supported by 2 bearings, which are SKF roller bearing on the drive-end side and roller bearing on the valve side and the engineering specifications of the bearing, which are described in Table 4. During the rotating, there is a friction torque from the bearing, however, the amplitudes are smaller significantly than the torque of the gearbox. Therefore, it is neglected in the analysis.

In the handling method by Mathcad, it is assumed that the supports are located at the center of the bearing.

In SolidWorks Simulation, the bearings are presented by fixtures. The cylinder face fixtures are applied on the faces where the bearings are assembled on the shaft. In order to carry out the research, it is necessary to assume that the fixture on the valve side is fixed in the axial direction and unable to rotate. Because of the properties of the bearing, both fixtures are not allowed to expand. Depending on those, the translations of the fixture and the example of fixtures in Simulation are shown in Table 5 and Figure 16, respectively. Translations which include are radial, axial, and circumferential are the maximum ranges that the fixture is allowed to deform. If the translation is equal to 0, the fixture will be fixed in that direction.

Bearing	Drive-end side	Valve side
Modal code	22218 CCK/W33	
Distance from the end of valve side (mm)	243.5	2324
Width (mm)	80	40

Table 4. The specifications of the bearing

Translations	Valve side	Drive-end side
Radial	0	0
Circumferential	0	None

Axial	0	None
-------	---	------

Table 5. The translations of the fixtures

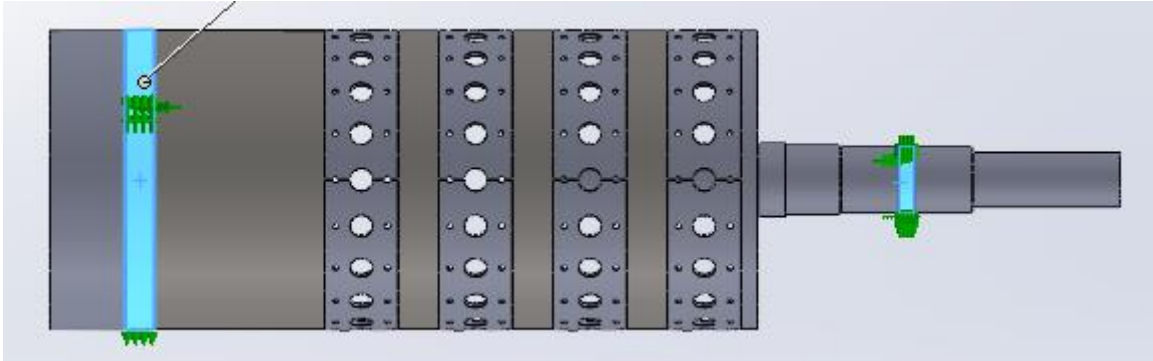


Figure 16. The fixtures in 4-disc-shaft static study

4.1.2 Disc

There are a number of discs assembled on the shaft, in which the minimum is 4 and the maximum is 26 discs. The 3D model and mass properties of the disc are shown in Figure 17 and Figure 18, respectively. Because the disc is an asymmetric assembled from the sectors and sector holders, the mass center of the disc coincides with the center of the cylinder face which is formed by the footplates.

In the handling method, it is assumed that the discs uses a gravity force which is located at the center of these. The gravity force of the disc that applies to the shaft is calculated by the formula (46).

$$F_d = m_d * g \quad (46)$$

where:

$m_d = 363.3 \text{ kg}$: Mass of disc

$g = 9.81$: Gravity coefficient

In SolidWorks Simulation, the discs are replaced by the 'remote loads', which are applied on the face of the footplate attached with the vat. Moreover, the centers of the remote loads are located on the central axis of the shaft and the moments of the inertia taken at the center of the disc are added with the same coordinate system of the disc. The example of remote loads which replace the disc in SolidWorks Simulation is shown in Figure 19.

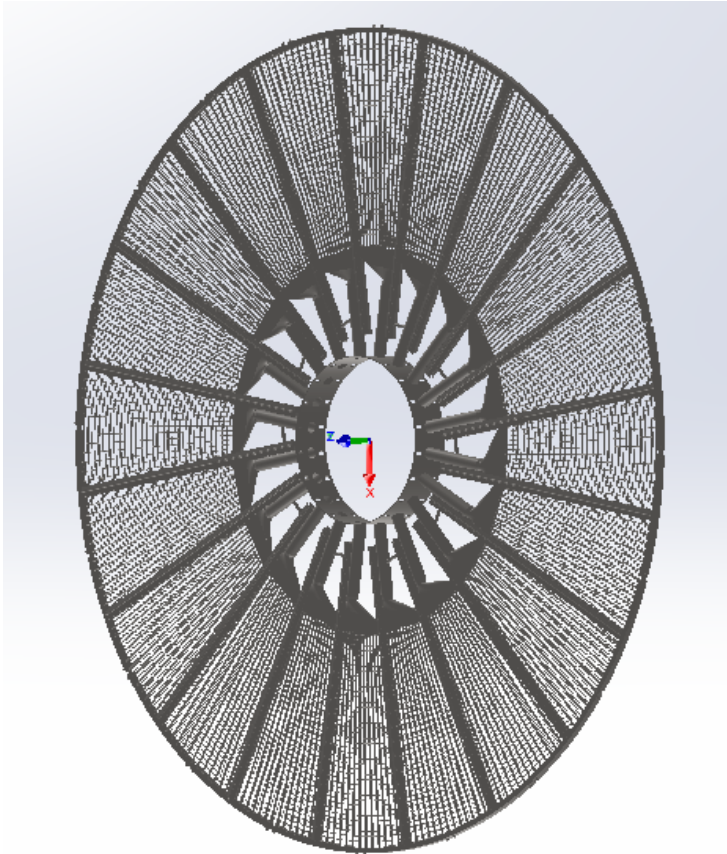


Figure 17. 3D model of the disc

Mass properties of Disc		
Configuration: Default		
Coordinate system: -- default --		
Mass = 363317.60 grams		
Volume = 45414699.82 cubic millimeters		
Surface area = 40301877.11 square millimeters		
Center of mass: (millimeters)		
X = 1125.13		
Y = 243.94		
Z = 2120.49		
Principal axes of inertia and principal moments of inertia: (grams * square millimeters)		
Taken at the center of mass.		
Ix = (1.00, 0.00, 0.00)	Px = 324486243360.24	
Iy = (0.00, 1.00, 0.00)	Py = 324486243360.24	
Iz = (0.00, 0.00, 1.00)	Pz = 648764864483.89	
Moments of inertia: (grams * square millimeters)		
Taken at the center of mass and aligned with the output coordinate system.		
Lxx = 324486243360.24	Lxy = 0.00	Lxz = 0.00
Lyx = 0.00	Lyy = 324486243360.23	Lyz = 0.00
Lzx = 0.00	Lzy = 0.00	Lzz = 648764864483.89
Moments of inertia: (grams * square millimeters)		
Taken at the output coordinate system.		
lxx = 1979757093479.98	lxy = 99718778021.59	lxz = 866809312253.77
lyx = 99718778021.59	lyy = 2418062657777.46	lyz = 187937085653.53
lzx = 866809312253.77	lzy = 187937085653.53	lzz = 1130311442142.40

Figure 18. The mass property of the disc

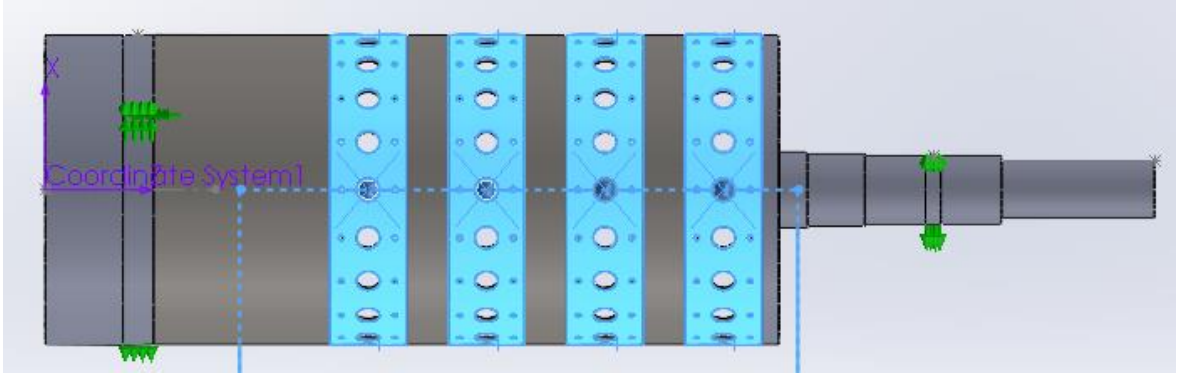


Figure 19. The remote loads in 4-disc-shaft static study

4.1.3 The tubes

There are 20 tubes which are also called channels that are placed inside the shaft and supported by 3 plates that are welded inside the vat (Figure 20 and 21 in Appendix 1). In order to simplify the analysis, the weights of the channels are replaced by the forces which contributes to support plates, which are equal to the reaction forces of the plates according to the third Newton's law. The free-body diagram of the channel is show in Figure 22 and it is assumed that the supports are located at the middle of the plate. Because there are 3 supports, the 3-moment-equations method is applied to handle the reaction forces.

It is clear from the FBD of the channels that the distance between the plates and the ends of the channels are constant, which are 12.5 and 550 mm. As a result, depending on the number of discs, the length of the channel (L_c) is different. The tube is divided into 2 parts, which are AB (1) and BC (2) and the bending diagram of each part in 2-support-systems is drawn in Figure 23. The 3-moment-equation is written in the form:

$$\frac{M_A * L_1}{E_1 * I_1} + 2 * M_B * \left(\frac{L_1}{E_1 * I_1} + \frac{L_2}{E_2 * I_2} \right) + \frac{M_C * L_2}{E_2 * I_2} = \frac{-6 * A_1 * x_1}{E_1 * I_1 * L_1} + \frac{-6 * A_2 * x_2}{E_2 * I_2 * L_2} \quad (47)$$

where:

$M_A = q * (12.5 \text{ mm})^2$: Bending moment at point A

M_B : Bending moment at point B

$M_C = 0$: Bending moment at point C

$q = \frac{m_c * 9.81}{L_c}$: Distributed load of the channel

m_c : The mass of the channel

$L_2 = 550 \text{ mm}$: Distance between the supports B and C

$L_1 = L_c - L_2$: Distance between the supports A and B

L_c : The length of the channel

E_1, E_2 : Elastic modulus

I_1, I_2 : Moment of inertia

$$A_1 = \frac{2}{3} * w_1 * \frac{L_1}{8} * L_1$$

$$A_2 = \frac{2}{3} * w_2 * \frac{L_2}{8} * L_2$$

$$w_1 = q * L_1$$

$$w_2 = q * L_2$$

$$x_1 = \frac{L_1}{2}$$

$$x_2 = \frac{L_2}{2}$$

It is assumed that the channel is a pipe without any holes in the body, so the cross-section area of the channel is constant. Therefore, the elastic module and moment of inertia of 2 parts AB and BC are equal. The equation (47) becomes equation (48)

$$M_A * L_1 + 2 * M_B * (L_1 + L_2) + M_C * L_2 = \frac{-6 * A_1 * x_1}{L_1} + \frac{-6 * A_2 * x_2}{L_2} \quad (48)$$

$$\Leftrightarrow M_B = \frac{\frac{-6 * A_1 * x_1}{L_1} + \frac{-6 * A_2 * x_2}{L_2} - M_A * L_1 - M_C * L_2}{2 * (L_1 + L_2)} \quad (49)$$

The FBD of each span with the virtual cut is shown in Figure 24 and the moment equilibrium equations and point A, B which are on both right and left side, and C are formed to calculate the shearing forces at those points. The reaction force at point A, B, and C are calculated by the formulas (53), (58), and (55), respectively.

$$CCW \sum M_A = M_A - M_B - q * L_1 * \frac{L_1}{2} - V_{B1} * L_1 = 0 \quad (50)$$

$$\Leftrightarrow V_{B1} = \frac{M_A - M_B - q * L_1 * \frac{L_1}{2}}{L_1} \quad (51)$$

$$CCW \sum M_B = M_A - M_B + q * L_1 * \frac{L_1}{2} - V_A * L_1 = 0 \text{ (Right side) (52)}$$

$$\leftrightarrow V_A = \frac{M_A - M_B + q * L_1 * \frac{L_1}{2}}{L_1} \text{ (53)}$$

$$CW \sum M_B = M_C - M_B + q * L_2 * \frac{L_2}{2} + V_C * L_2 = 0 \text{ (Left side) (54)}$$

$$\leftrightarrow V_C = \frac{M_C - M_B + q * L_2 * \frac{L_2}{2}}{L_2} \text{ (55)}$$

$$CW \sum M_C = M_C - M_B - q * L_2 * \frac{L_2}{2} + V_{B2} * L_2 = 0 \text{ (56)}$$

$$\leftrightarrow V_{B2} = \frac{-M_C + M_B + q * L_2 * \frac{L_2}{2}}{L_2} \text{ (57)}$$

$$V_B = |V_{B2} - V_{B1}| \text{ (58)}$$

$$F_A = 20 * V_A \text{ (59)}$$

$$F_B = 20 * V_B \text{ (60)}$$

$$F_C = 20 * V_C \text{ (61)}$$

According to the third Newton's law, the forces that the channels apply to the support plates are equal to the reaction forces in opposite directions.

In the handling method, it is assumed that the forces of 20 channels which affect each support plate are combined into 3 forces which are located at the middle of the plates. The amplitudes of those are equal to 20 times the reaction forces at the plates and in the same direction which are calculated by formulas (59), (60), and (61).

In FEM by SolidWorks, the channels are omitted and described by the forces. Those forces applied on the faces of the plates where the channels are attached. The example of the forces of channels applied to the support plate which is on the valve side is shown in Figure 25 of Appendix 1.

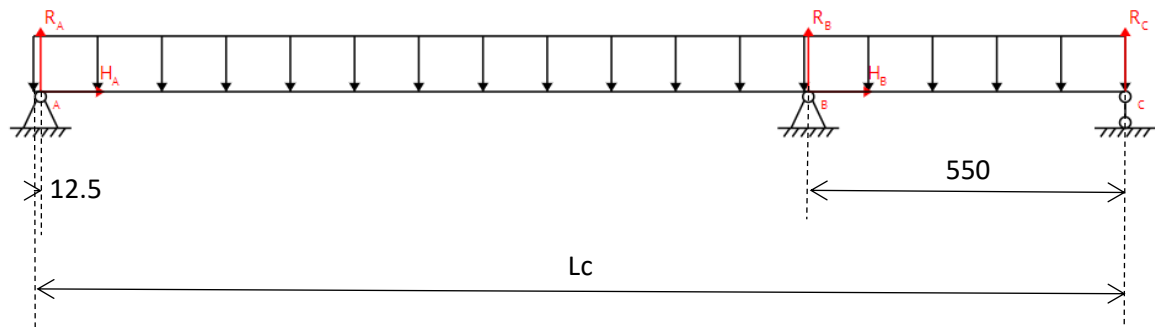


Figure 22. Free-body-diagram of the channels

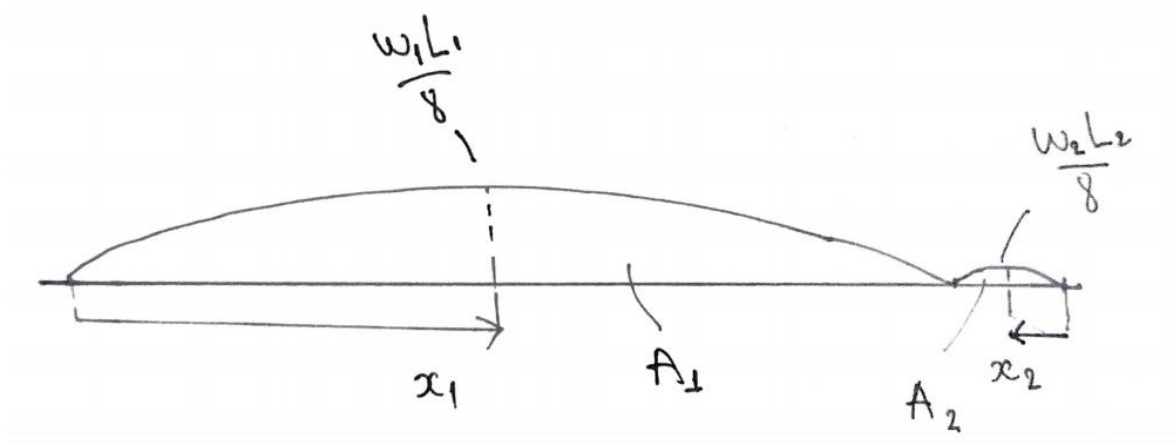


Figure 23. The bending diagrams of each part if in simple supports system

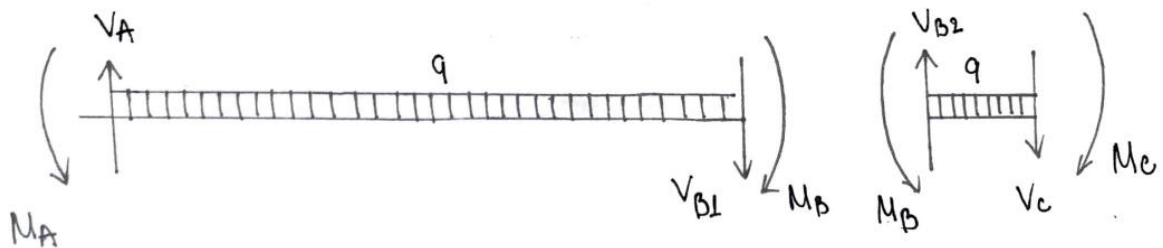


Figure 24. Free Body Diagram of each span with virtual cut

4.1.4 Gearbox

The shaft is rotated by the gearbox which is the model M4PHT50. The gearbox is assembled with the 149-millimeter-drive end part, therefore, there is a force, which caused by the weight of the gearbox, applies at the end of the drive end. Moreover, the gearbox causes a continuous torque, which is calculated by the formulas (63), at the drive end. The initial information of the gearbox, which is researched from the SEW catalogue, is shown in the Table 6. At the beginning of the operation, the maximum power is applied, hence, the shaft

is restricted to the biggest torque which the initial values and the calculation are shown in the Figure 26.

$$\tau_i = \frac{P}{n} \quad (62)$$

$$\tau_o = i_g * i_b * \tau_i \quad (63)$$

where:

τ_i : Input torque

P : Power of the motor

n : The rotating speed of the shaft

τ_o : Output torque

$i_g = 400$: Gearbox ratio

$i_b = 2.5$: Belt ratio

In handling calculations, assuming that the gravity force that the gearbox applies is located at the beginning point of the shaft and it is calculated by the formula (64).

$$F_g = m_g * g \quad (64)$$

where:

m_g : the weight of the gearbox.

$g = 9.81$: gravity coefficient

In the FEM, the example of the torque which is caused by the gearbox applied to the shaft is shown in Figure 27 and the weight of the gearbox is present as the 'distribute mass' on the end face of the drive end which is shown in Figure 28.

Model	M4PHT50
Mass	845 kilogram
Power	4.5 Watt. 7.5 Watt
Rotating speed	960 rpm, 1450 rpm
Gear ratio	400

Belt ratio	2.5
------------	-----

Table 6. The initial information of the gearbox

$$\begin{aligned}
 P &= 7.5 \text{ kW} \\
 n &:= 960 \text{ rpm} \\
 T_i &:= \frac{P}{n} = 74.604 \text{ N}\cdot\text{m} \\
 i_g &:= 400 \quad i_b := 2.5 \\
 T_o &:= T_i \cdot i_g \cdot i_b = 74603.88 \text{ N}\cdot\text{m}
 \end{aligned}$$

Figure 26. The calculation of the gearbox torque.

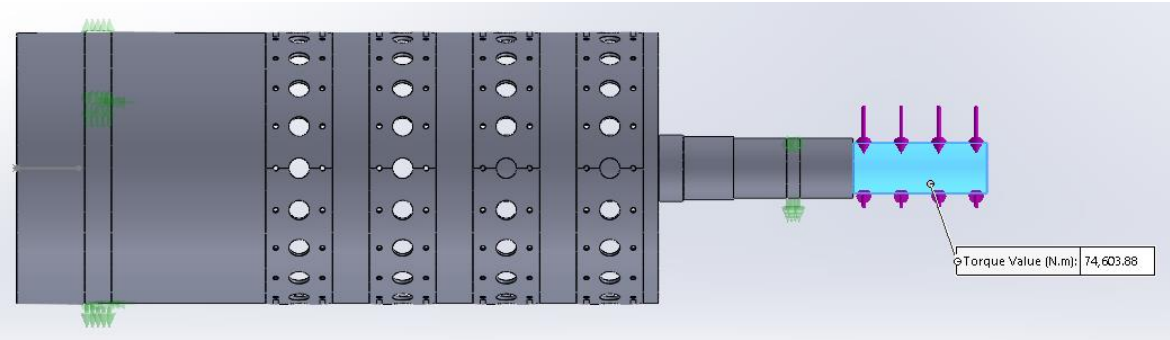


Figure 27. The torque of the gearbox applies to the 4-disc-shaft.

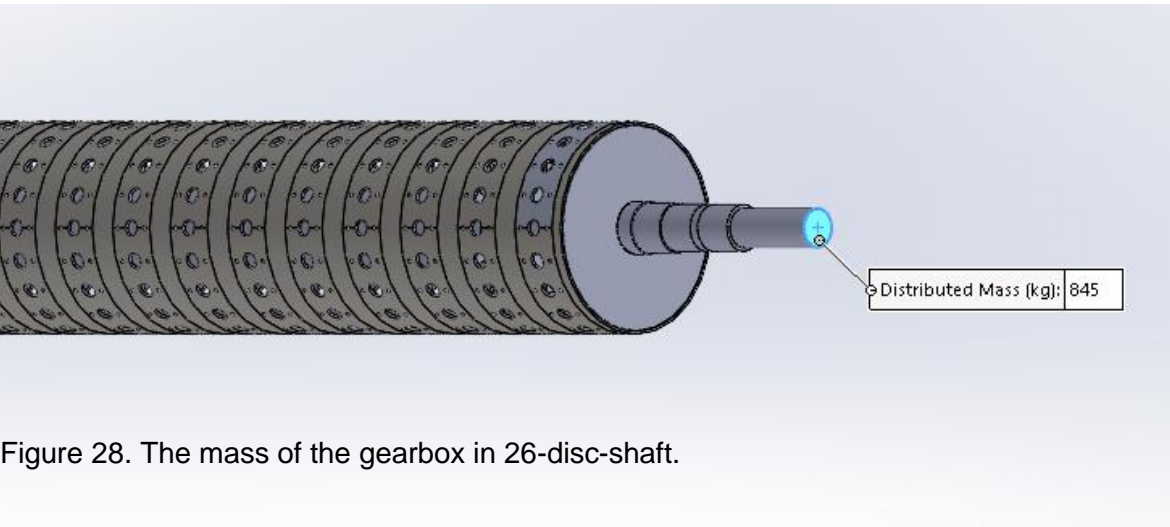


Figure 28. The mass of the gearbox in 26-disc-shaft.

4.1.5 Water

The shaft is submerged partly into the water during the operation. The distance between the water level and the center of the shaft is 750 mm. As a result, there is a force from water, which is applied on the shaft in the opposite direction with the gravity. Nevertheless, this force is neglected because it is too small to compare to others and affects lightly to the shaft. In addition, when the shaft is rotating, there is a torque restricting the motion, caused by water. Most of the restrictions are applied to the discs, so it is assumed that the torque is distributed equally on the discs. Moreover, the sum of amplitude of the torques on each disc is equal and in the reverse direction to the torque caused by the gearbox.

In the handling method, the drive end is the part that takes the largest amplitude of the twist.

In SolidWorks Simulation, because the disc is submerged partly into the water, it is assumed that the torques are added in the hollow part of the shaft on the face where the footplates of the disc are attached. Moreover, the amplitude is equal in the opposite direction to the torque of the gearbox and the 'Total' box is ticked. The example of the torque caused by the water is shown in Figure 29 in Appendix 1.

4.2 4-disc-shaft

4.2.1 Handling method by Mathcad

The free body diagram of the 4-disc-shaft is shown in Figure 33. It is clear from the FBD that there are 2 supports which present 2 bearings. The gravity force of the disc is calculated by the formula (46) and described by P_5, P_6, P_7, P_8 . The mass of the gearbox is added at the end of the shaft and calculated by the formula (64) and demonstrated by P_1 . The forces applied by the support plates are then calculated by the formulas (59), (60) and (61) and signed by P_2, P_3, P_4 in the FBD, in turn.

The equilibrium equations are applied to solve the reaction forces.

$$\begin{cases} \text{CCW} \sum M_A = 0 & (65) \\ \uparrow \sum F_y = 0 & (66) \end{cases}$$

$$\leftrightarrow \begin{cases} P_2 * 243.5 - P_5 * 601.5 - P_6 * 911.5 - P_3 * 1094 - P_7 * 1221.5 - P_8 * 1531.5 \\ \quad + P_4 * 1676.5 + R_B * 2080.5 - P_1 * 2659.5 = 0 & (67) \\ R_A + P_4 + R_B - P_2 - P_5 - P_6 - P_3 - P_7 - P_8 - P_1 = 0 & (68) \end{cases}$$

↔

$$\begin{cases} R_B = \left(\begin{array}{c} -P_2 * 243.5 + P_5 * 601.5 + P_6 * 911.5 + P_3 * 1094 + P_7 * 1221.5 + P_8 * 1531.5 \\ -P_4 * 1676.5 + P_1 * 2659.5 \end{array} \right) / 2080.5 \quad (69) \\ R_A = -P_4 - R_B + P_2 + P_5 + P_6 + P_3 + P_7 + P_8 + P_1 \quad (70) \end{cases}$$

Firstly, the forces of the inner channels and the forces by the support plates that are applied on the shaft are calculated by MathCad in Figure 31. Moreover, the initial values in the calculation are shown in Figure 30. Hence, the number of the applied formulas are noted after each calculation.

After that, the values of the forces including gravity forces of gearbox and disc, are imported into the MathCad which is shown in Figure 32. Base on the formulas (69) and (70) the reactions at the bearings A and B are calculated in Figure 37, the shearing force and bending diagram of the shaft is drawn in Figure 34 and 35.

In the stress calculation, the torque takes the significant value, therefore, the drive-end is the part that takes the maximum Von Mises stress. The most critical point on the shaft is the connection between the 149 mm and 180 mm diameter parts which is shown in Figure 36. The Von Mises stress of this point is determined. As a result, depending on the shearing force diagram and bending diagram, the bending moment is calculated by the formula (71), and the shearing force at the point is determined.

$$M_b = V * d \quad (71)$$

where:

M_b : The bending moment at the critical point

$V = 8289 \text{ N}$: Shearing force at the point

$d = 400 \text{ mm}$: The distance between the point and the end of drive end

The initial values of the moment, force, and torque are imported into the MathCad which is shown in Figure 38. The bending stress, torque stress and are calculated by the formulas (72) and (73) in turn which are determined in Figure 38. The direct shearing stress in the upper and lower point of the shaft is equal to 0. The Von Mises stress and the safety factor with the tensile strength of 400 MPa are calculated by the formula (74) and (75).

$$\sigma_b = \frac{M_b}{\frac{d^3}{32} * \pi} \quad (72)$$

$$\tau = \frac{T}{\frac{d^3}{32} * \pi} \quad (73)$$

$$\sigma_v = \sqrt{((\sigma_b + \sigma_t))^2 + 3 * (\tau + \sigma_s)^2} (74)$$

$$n = \frac{Re}{\sigma_v} (75)$$

$$L_c := 1895 \text{ mm}$$

$$m_c := 11.93287 \text{ kg}$$

$$L_2 := 550 \text{ mm}$$

$$L_1 := L_c - L_2 = 1.345 \text{ m}$$

$$q := \frac{m_c \cdot 9.81 \frac{N}{kg}}{L_c} = 0.062 \frac{N}{mm}$$

$$w_1 := q \cdot L_1 = 83.086 \text{ N}$$

$$w_2 := q \cdot L_2 = 33.976 \text{ N}$$

$$x_1 := \frac{L_1}{2}$$

$$x_2 := \frac{L_2}{2}$$

$$A_1 := \frac{2}{3} \cdot w_1 \cdot \frac{L_1}{8} \cdot L_1 = (1.253 \cdot 10^7) \text{ N} \cdot \text{mm}^2$$

$$A_2 := \frac{2}{3} \cdot w_2 \cdot \frac{L_2}{8} \cdot L_2 = (8.565 \cdot 10^5) \text{ N} \cdot \text{mm}^2$$

$$M_A := q \cdot \frac{25}{2} \text{ mm} \cdot 25 \text{ mm}$$

$$M_C := 0 \text{ N} \cdot \text{m}$$

Figure 30. The inertial values of inner channel calculation

$$M_b := \frac{\left(-6 \cdot A_1 \cdot \frac{x_1}{L_1} - 6 \cdot A_2 \cdot \frac{x_2}{L_2} - L_1 \cdot M_A - L_2 \cdot M_C\right)}{2 (L_1 + L_2)} = -1.06 \cdot 10^4 \text{ N} \cdot \text{mm} \quad (49)$$

$$M_B := -M_b$$

$$V_{B1} := \frac{M_A - M_B - q \cdot L_1 \cdot \frac{L_1}{2}}{L_1} = -49.409 \text{ N} \quad (51)$$

$$V_A := \frac{-M_B + q \cdot L_1 \cdot \frac{L_1}{2}}{L_1} = 33.662 \text{ N} \quad (53)$$

$$V_C := \frac{M_B - q \cdot \frac{L_2}{2} \cdot L_2}{L_2} = 2.284 \text{ N} \quad (55)$$

$$V_{B2} := \frac{M_B + q \cdot L_2 \cdot \frac{L_2}{2}}{L_2} = 36.259 \text{ N} \quad (57)$$

$$V_B := V_{B2} - V_{B1} = 85.668 \text{ N} \quad (58)$$

$$F_A := V_A \cdot 20 = 673.247 \text{ N} \quad (59)$$

$$F_B := 20 \cdot V_B = 1713.369 \text{ N} \quad (60)$$

$$F_C := 20 \cdot V_C = 45.674 \text{ N} \quad (61)$$

Figure 31. The inner channel calculation

$m_g := 845 \text{ kg}$	$m_d := 363.3 \text{ kg}$
$F_g := m_g \cdot 9.81 \frac{\text{N}}{\text{kg}} = (8.289 \cdot 10^3) \text{ N} \quad (64)$	$F_d := m_d \cdot 9.81 \frac{\text{N}}{\text{kg}} = (3.564 \cdot 10^3) \text{ N} \quad (46)$
$P_1 := F_g = 8289.45 \text{ N}$	$P_4 := F_C = 45.674 \text{ N}$
	+
$P_3 := F_B = 1713.369 \text{ N}$	$P_5 := F_d = 3563.973 \text{ N}$
$P_2 := F_A = 673.247 \text{ N}$	$P_6 := P_5$
	$P_7 := P_5$
	$P_8 := P_5$

Figure 32. The initial values of shaft calculation

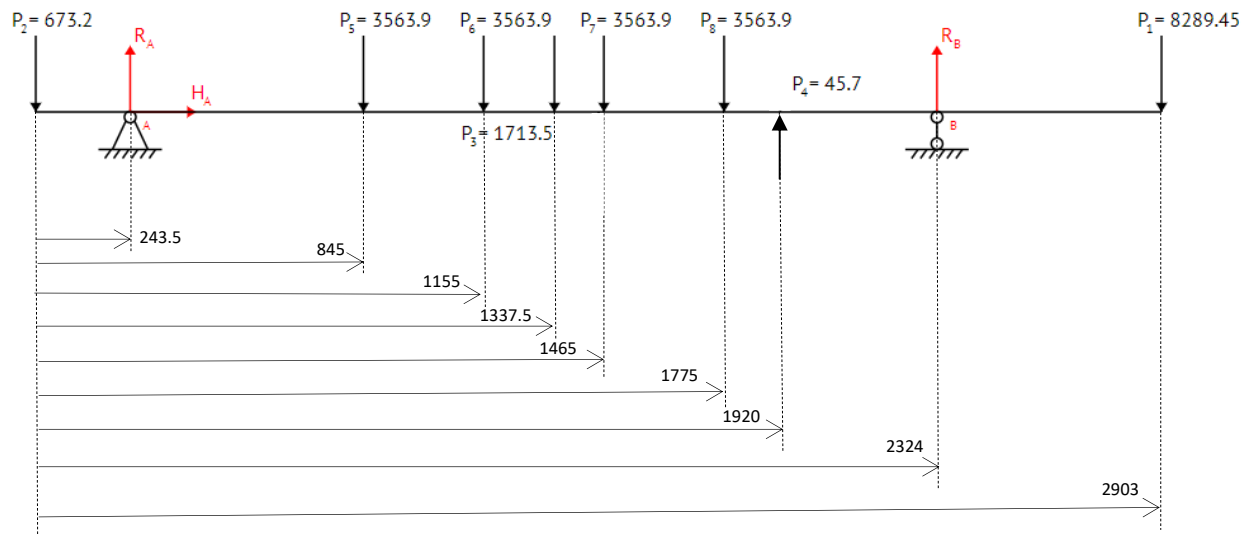


Figure 33. The Free body diagram of the 4-disc-shaft

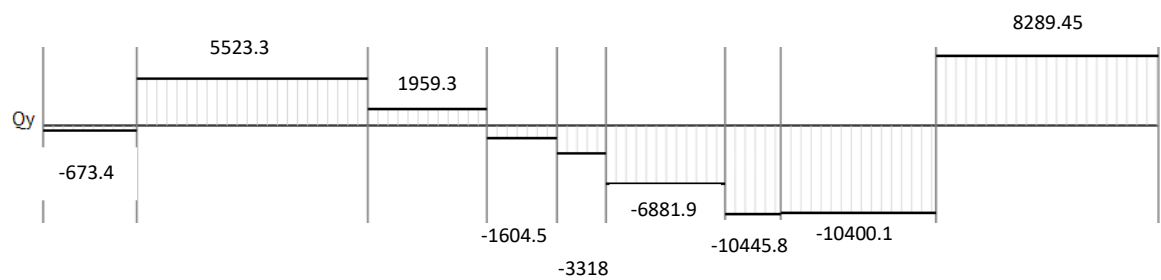


Figure 34. The shearing force diagram of 4-disc-shaft in Newton

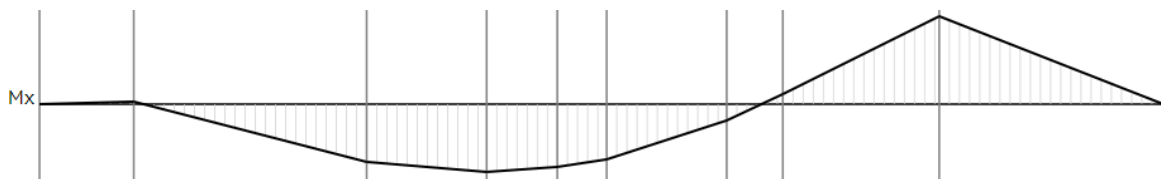


Figure 35. The bending diagram of the 4-disc-shaft.

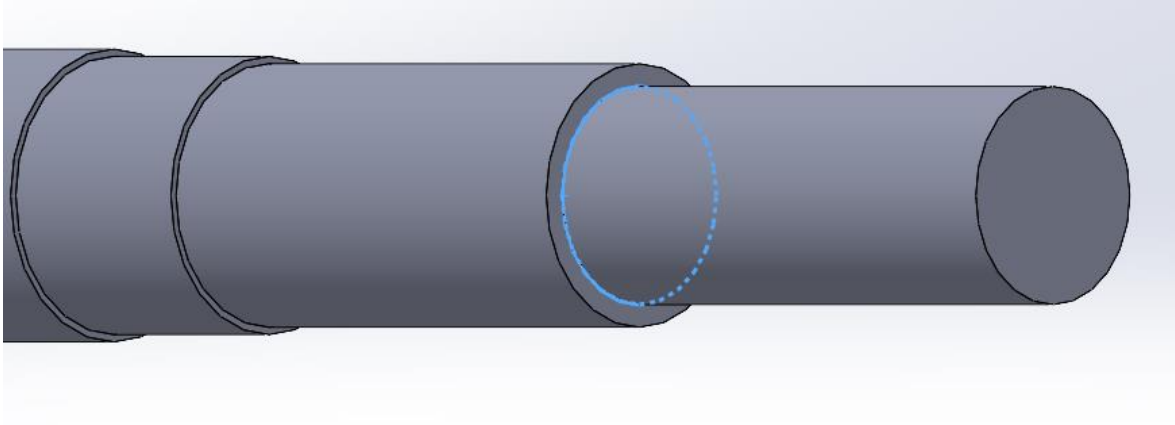


Figure 36. The most critical point on the shaft.

$$R_B := \frac{-P_2 \cdot 243.5 + P_5 \cdot 601.5 + P_6 \cdot 911.5 + P_3 \cdot 1094 + P_7 \cdot 1221.5 + P_8 \cdot 1531.5 - P_4 \cdot 1676.5 + P_1 \cdot 2659.5}{2324 - 243.5} = (1.869 \cdot 10^4) \text{ N} \quad (69)$$

$$R_A := P_2 + P_5 + P_6 + P_3 + P_7 + P_8 + P_1 - P_4 - R_B = 6196.73 \text{ N} \quad (70)$$

Figure 37. The reactions calculation of the 4-disc-shaft.

$$\sigma_s := 0 \text{ MPa} \quad \sigma_t := 0 \text{ MPa} \quad d := 149 \text{ mm} \quad Re := 400 \text{ MPa}$$

$$M_b := P_1 \cdot 400 \text{ mm} = (3.316 \cdot 10^3) \text{ N} \cdot \text{m} \quad (71)$$

$$\sigma_b := \frac{M_b}{\frac{d^3}{32} \cdot \pi} = 10.21 \text{ MPa} \quad (72)$$

$$\tau := \frac{T_{shaft}}{\frac{d^3}{16} \cdot \pi} = 84.231 \text{ MPa} \quad (73)$$

$$\sigma_v := \sqrt{(\sigma_b + \sigma_t)^2 + 3 \cdot (\tau^2 + \sigma_s^2)} = 146.25 \text{ MPa} \quad (74)$$

$$n := \frac{Re}{\sigma_v} = 2.735 \quad (75)$$

Figure 38. The stresses and safety factor calculation.

4.2.2 FEM by SolidWorks Simulation

The features are added to the study including fixtures, masses of the disc, the mass of the gearbox, torques by the gearbox, and water. The values are shown in heading 2.1. There are 2 studies in which the difference is the presence of the inner channels. In the first study, the channels are replaced by forces that are applied on the support plate (Figure 40 in Appendix 1) which is described in heading 2.1.3, and the values are shown in Figure 31. By

contrast, in the other study, the channels are replaced by the remoted loads which are applied on the attached faces between them and the shaft (Figure 41 in Appendix 1). The mass property of the channel, including the central mass and the moment of inertia, is shown in Figure 39. The stress results of the first and second studies are shown in Figure 42 and 43, respectively. The results between the 2 studies are slightly different, which are caused by the number tolerance. It can be concluded that replacing the mass of the inner channel with force is correct.

```

Mass properties of Tube_upp_310mm_4 disc
Configuration: Default
Coordinate system: -- default --

Density = 0.01 grams per cubic millimeter

Mass = 11932.87 grams

Volume = 1491608.38 cubic millimeters

Surface area = 1494826.18 square millimeters

Center of mass: ( millimeters )
X = 0.00
Y = 0.85
Z = 942.51

Principal axes of inertia and principal moments of inertia: ( grams * square millimeters )
Taken at the center of mass.
Ix = ( 0.00, 0.00, 1.00)   Px = 48117426.21
Iy = ( 1.00, 0.00, 0.00)   Py = 3602213143.66
Iz = ( 0.00, 1.00, 0.00)   Pz = 3602822479.76

Moments of inertia: ( grams * square millimeters )
Taken at the center of mass and aligned with the output coordinate system.
Lxx = 3602213153.17      Lxy = 2401.37      Lxz = -10342.56
Lyx = 2401.37           Lyy = 3602818538.04   Lyz = 3738674.36
Lzx = -10342.56         Lzy = 3738674.36     Lzz = 48121358.41

```

Figure 39. The mass property of the 4-disc-inner channel.

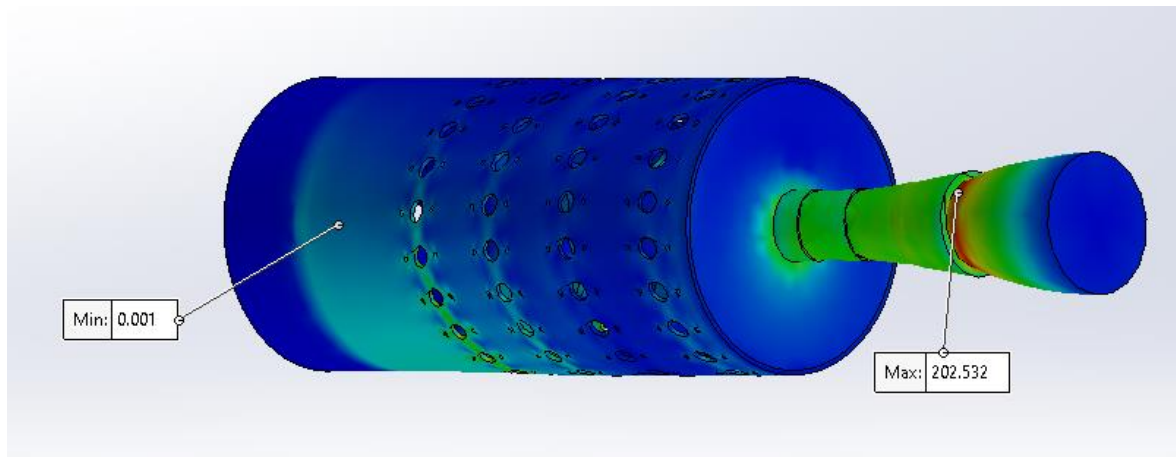


Figure 42. The Von mise stress plot of first study of 4-disc shaft.

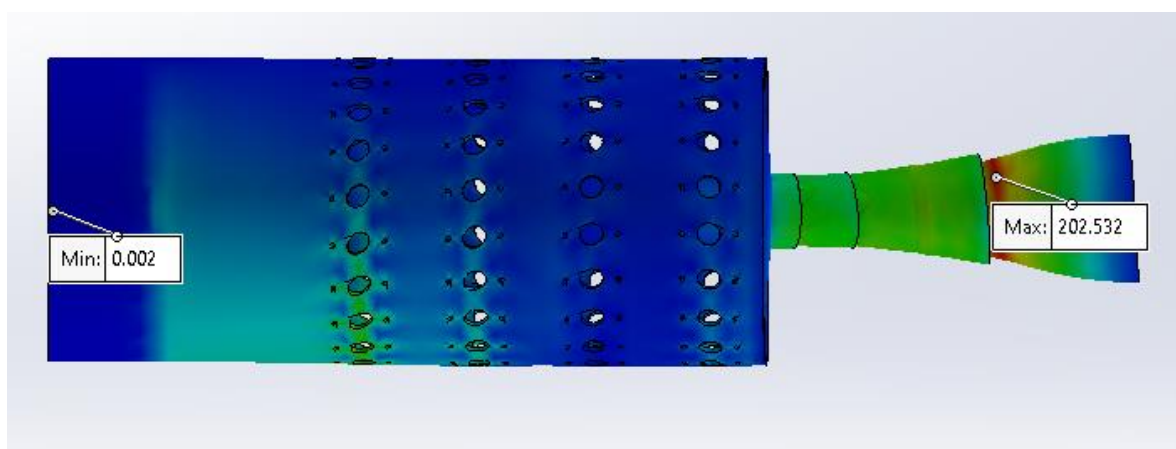


Figure 43. The Von mise stress plot of second study of 4-disc shaft.

4.2.3 Conclusion

It can be seen that there is a mild difference in the results of the 2 methods, which is generated by the notch factors that are only accounted in FEM by Simulation. The 4-disc-calculation is used to explain the static analysis, the 26-disc-shaft is the critical model. Moreover, it shown that the FEM by Simulation gives the correct results compared to the traditional method. Hence, only the FEM method and 26-disc-shaft are applied in the developing phase to save time for the thesis.

4.3 26-disc-shaft

4.3.1 Handling method

The method that is applied to calculate the reaction forces of the inner channels of the plate, the reaction force at the bearing is the same as the 4-disc-shaft. The calculation of the forces that the inner channels apply on the support plate is shown in Figure 44. Because there are 26 discs that cause difficulty in the calculation, the combined force is replaced.

The magnitude of the combined force is 26 times the mass of one disc and located at the central of 26 discs. Thus, this method will lead to the error in shearing force and bending diagram of the shaft, but the main purpose is finding the peak of the diagram which remains correct. The initial values, FBD, and reaction calculation of 26-disc-shaft are shown in Figure 46, 45 and 47, respectively. Depending on the shearing force and bending diagrams (described in the Figure 47), that the stresses at the critical point is located on the drive end is calculated in Figure 30.

$$\begin{aligned}
L_c &:= 8715 \text{ mm} & m_c &:= 54.53619 \text{ kg} \\
L_2 &:= 300 \text{ mm} \\
L_1 &:= L_c - L_2 = 8.415 \text{ m} & q &:= \frac{m_c \cdot 9.81 \frac{\text{N}}{\text{kg}}}{L_c} = 0.061 \frac{\text{N}}{\text{mm}} \\
w_1 &:= q \cdot L_1 = 516.583 \text{ N} & w_2 &:= q \cdot L_2 = 18.417 \text{ N} \\
x_1 &:= \frac{L_1}{2} & x_2 &:= \frac{L_2}{2} \\
A_1 &:= \frac{2}{3} \cdot w_1 \cdot \frac{L_1}{8} \cdot L_1 = (3.048 \cdot 10^9) \text{ N} \cdot \text{mm}^2 \\
A_2 &:= \frac{2}{3} \cdot w_2 \cdot \frac{L_2}{8} \cdot L_2 = (1.381 \cdot 10^5) \text{ N} \cdot \text{mm}^2 \\
M_A &:= q \cdot \frac{25}{2} \text{ mm} \cdot 25 \text{ mm} & M_C &:= M_A \\
M_b &:= \frac{\left(-6 \cdot A_1 \cdot \frac{x_1}{L_1} - 6 \cdot A_2 \cdot \frac{x_2}{L_2} - L_1 \cdot M_A - L_2 \cdot M_C \right)}{2 (L_1 + L_2)} = -524.71 \text{ N} \cdot \text{m} \\
M_B &:= -M_b \\
V_A &:= \frac{-M_B + q \cdot L_1 \cdot \frac{L_1}{2}}{L_1} = 195.938 \text{ N} \\
V_{B.L} &:= \frac{M_A - M_B - q \cdot L_1 \cdot \frac{L_1}{2}}{L_1} = -320.644 \text{ N} \\
V_C &:= \frac{M_B - q \cdot \frac{L_2}{2} \cdot L_2}{L_2} = 1739.824 \text{ N} \\
V_{B.R} &:= \frac{M_B + q \cdot L_2 \cdot \frac{L_2}{2}}{L_2} = (1.758 \cdot 10^3) \text{ N} \\
V_B &:= V_{B.R} - V_{B.L} = 2078.884 \text{ N}
\end{aligned}$$

Figure 44. The calculation of the force that the inner channels apply on the support plate

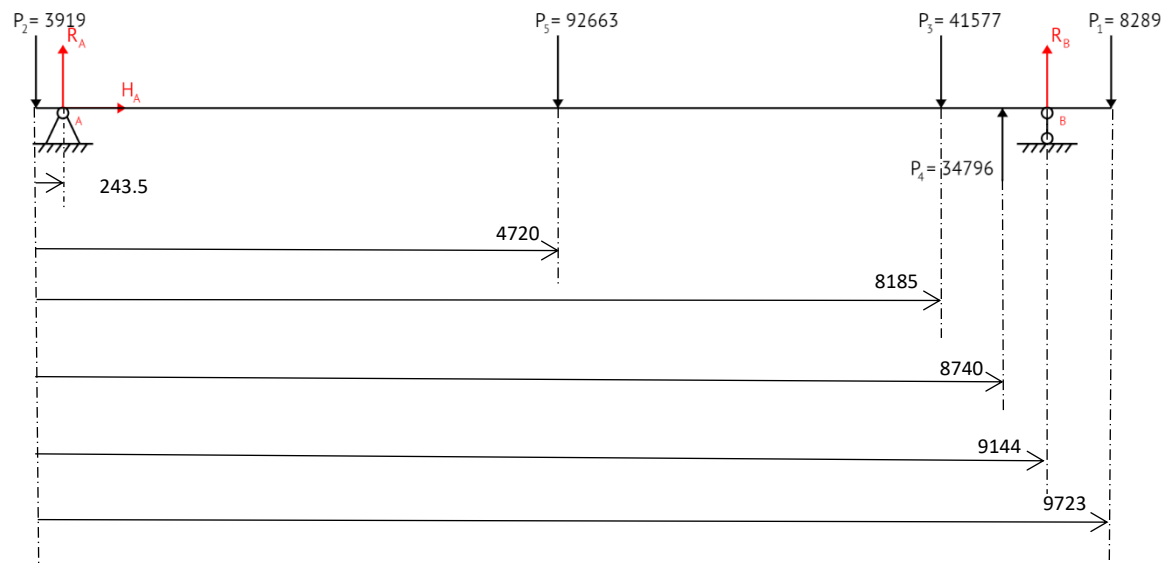


Figure 45. The FBD of the 26-disc-shaft.

$$\begin{aligned}
 m_d &:= 363.3 \text{ kg} & P_4 &:= 20 \cdot V_C = 34796.475 \text{ N} \\
 P_2 &:= 20 \cdot V_A = (3.919 \cdot 10^3) \text{ N} & P_5 &:= 26 \cdot m_d \cdot 9.81 \frac{\text{N}}{\text{kg}} = 92663.298 \text{ N} \\
 P_1 &:= m_g \cdot 9.81 \frac{\text{N}}{\text{kg}} = 8289.45 \text{ N} & P_3 &:= 20 \cdot V_B = 41577.676 \text{ N} \\
 R_B &:= \frac{-P_2 \cdot 243.5 + P_5 \cdot (4720 - 243.5) + P_3 \cdot (8185 - 243.5) - P_4 \cdot (8740 - 243.5) + P_1 \cdot (9723 - 243.5)}{9144 - 243.5} = (5.921 \cdot 10^4) \text{ N} \\
 R_A &:= P_1 + P_2 + P_3 - P_4 + P_5 - R_B = 52445.496 \text{ N}
 \end{aligned}$$

Figure 46. The reaction forces at the bearing of 26-disc-shaft.

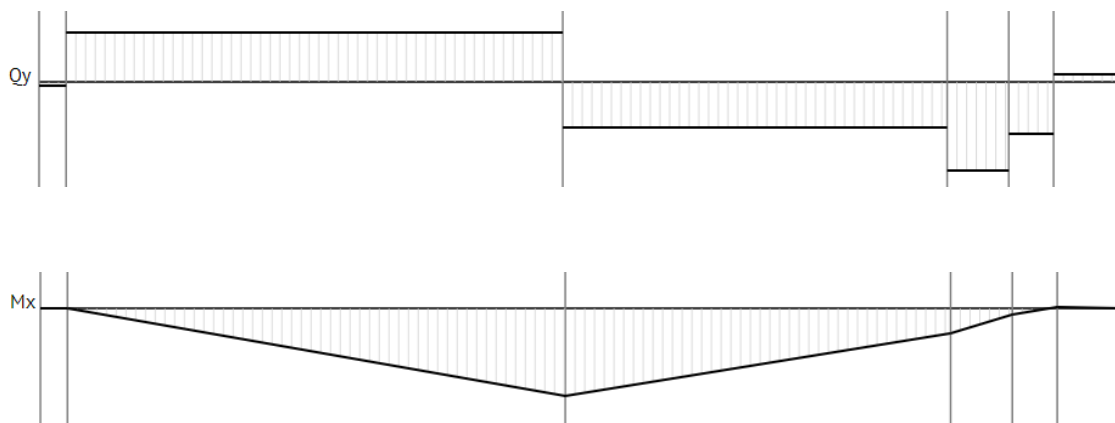


Figure 47. The shearing force and bending moment diagrams of 26-disc-shaft.

$$\sigma_s := 0 \text{ MPa} \quad \sigma_t := 0 \text{ MPa} \quad d := 149 \text{ mm} \quad Re := 400 \text{ MPa}$$

$$M_b := P_1 \cdot 400 \text{ mm} = (3.316 \cdot 10^3) \text{ N} \cdot \text{m} \quad (71)$$

$$\sigma_b := \frac{M_b}{\frac{d^3}{32} \cdot \pi} = 10.21 \text{ MPa} \quad (72)$$

$$\tau := \frac{T_{shaft}}{\frac{d^3}{16} \cdot \pi} = 84.231 \text{ MPa} \quad (73)$$

$$\sigma_v := \sqrt{(\sigma_b + \sigma_t)^2 + 3 \cdot (\tau^2 + \sigma_s^2)} = 146.25 \text{ MPa} \quad (74)$$

$$n := \frac{Re}{\sigma_v} = 2.735 \quad (75)$$

Figure 48. The stresses calculation of 26-disc-shaft.

4.3.2 FEM by SolidWorks Simulation

The study in which the channels are described as the forces applied on the plate is run and shown in Figure 50. The mass property of the inner channel in 26-disc-shaft is described in Figure 49.

```

Mass properties of Tube_upp_310mm_26 disc
Configuration: Default
Coordinate system: -- default --

Density = 0.01 grams per cubic millimeter

Mass = 54536.19 grams

Volume = 6817023.28 cubic millimeters

Surface area = 6834115.08 square millimeters

Center of mass: ( millimeters )
  X = -0.02
  Y = 1.25
  Z = 4349.62

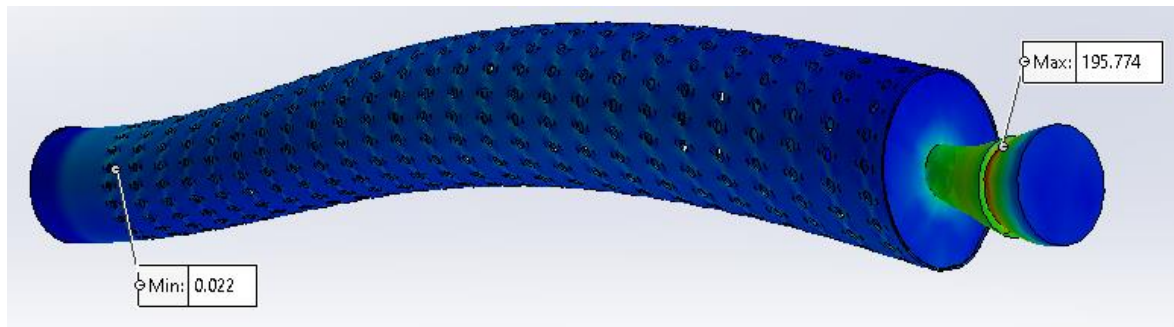
Principal axes of inertia and principal moments of inertia: ( grams * square millimeters )
Taken at the center of mass.
  lx = ( 0.00, 0.00, 1.00)    Px = 219946634.97
  ly = ( 1.00, 0.03, 0.00)   Py = 346206858755.04
  lz = (-0.03, 1.00, 0.00)   Pz = 346210986398.76

Moments of inertia: ( grams * square millimeters )
Taken at the center of mass and aligned with the output coordinate system.
  Lxx = 346206862331.27    Lxy = 121482.59    Lxz = -1628211.76
  Lyx = 121482.59         Lyy = 346210980651.13    Lyz = 27361151.39
  Lzx = -1628211.76       Lzy = 27361151.39    Lzz = 219948806.37

Moments of inertia: ( grams * square millimeters )
Taken at the output coordinate system.
  lxx = 1377988302030.51   lxy = 120019.39   lxz = -6735872.39
  lyx = 120019.39         lyy = 1377992335701.27   lyz = 322937608.95
  lzx = -6735872.39       lzy = 322937608.95   lzz = 220033506.03

```

Figure 49. The mass property of inner channel in 26-disc-shaft.



Fatigue 50. The Von mise stress plot of 26-disc-shaft

4.4 Conclusion

It can be seen from the calculation that the static safety factor of the 26-disc-shaft is about 2. The structure is strong enough to carry the loads and able to be developed by decreasing the dimension.

5 Deflection

5.1 Introduction

The rotating shaft, including the disc, is installed in a hood which is shown in Figure 51 of Appendix 1. Therefore, the deflection of the shaft needs to be tested to ensure that there is not any collision between them during the operation. In X and Z directions of the model, the clearance between the disc and the hood is equal to 80 mm which is shown in Figure 52 of Appendix 1. Each disc is located between 2 chutes where the cake formed during the operation. Hence in Y direction, the distance between the disc and the chute is 32.5 mm. Because the most critical model is 26-disc-shaft, the deflection plot of it is defined by Solid-Works Simulation.

5.2 Deflection of the 26-disc-shaft

The deflection plots of 26-disc-shaft in several directions are shown. In Figure 53, the deflection of the shaft in X and Z direction are shown, with the maximum magnitude of deflection being 2.198 mm. The maximum deflection of the shaft in the Y direction is 0.26mm. The deflection is smaller significantly than the allowable clearance, therefore it is ensured that there is any collision between the shaft and other components during the operation.

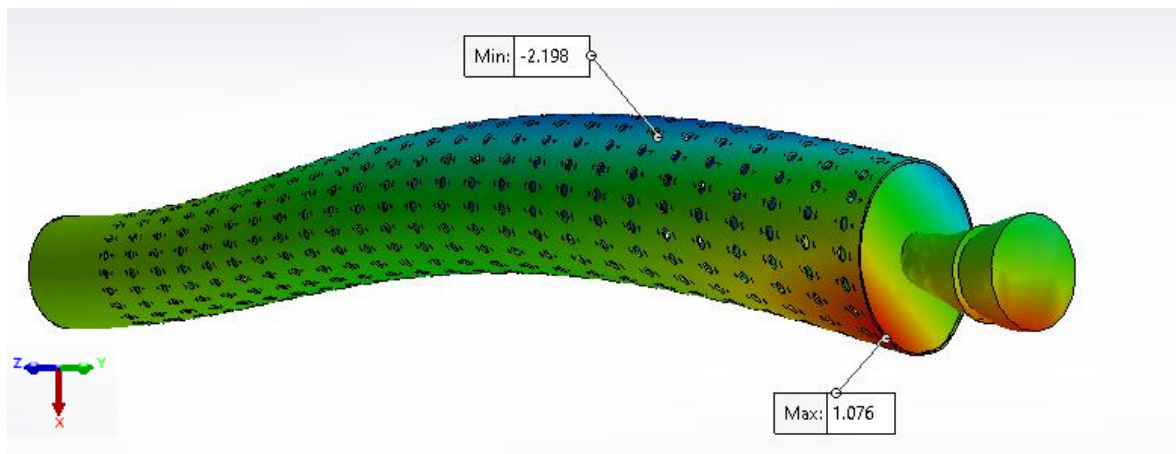


Figure 53. The deflection plot of 26-disc-shaft in X direction

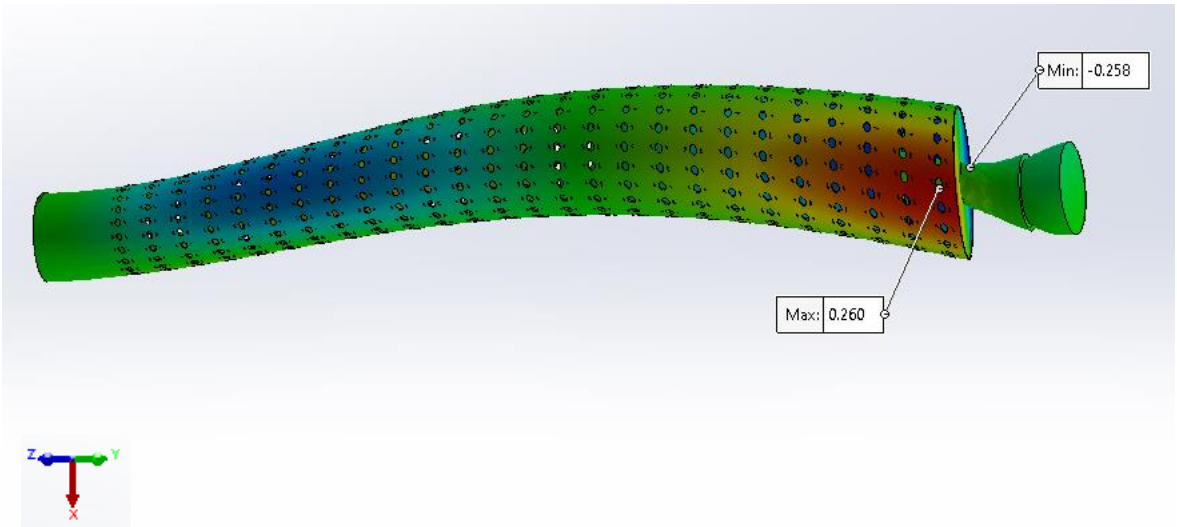


Figure 54. The deflection of 26-disc-sahft in Y direction

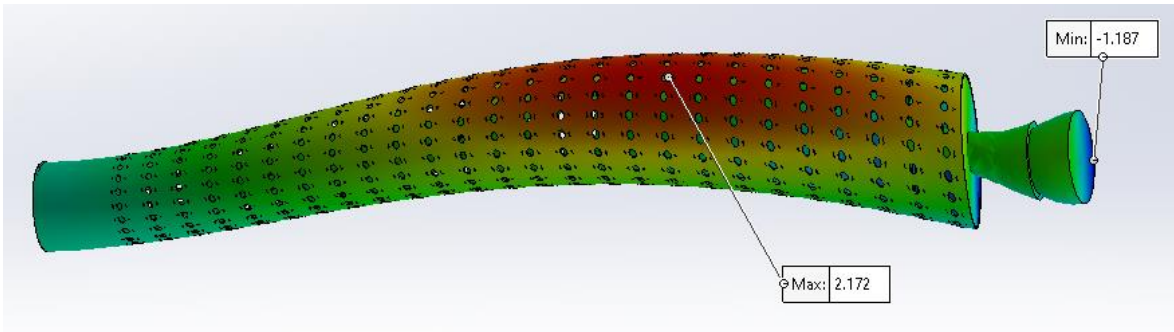


Figure 55. The deflection plot of 26-disc-shaft in Z direction

6 Fatigue calculation

6.1 Introduction

Fatigue is the important calculation in this model which is a rotating design. There are 2 critical points on the 26-disc-shaft where the fatigue strengths are defined which is shown in Figure 56. The stress-based infinite lifetime method is applied to define the stresses and it is assumed that there is any welding in that points.

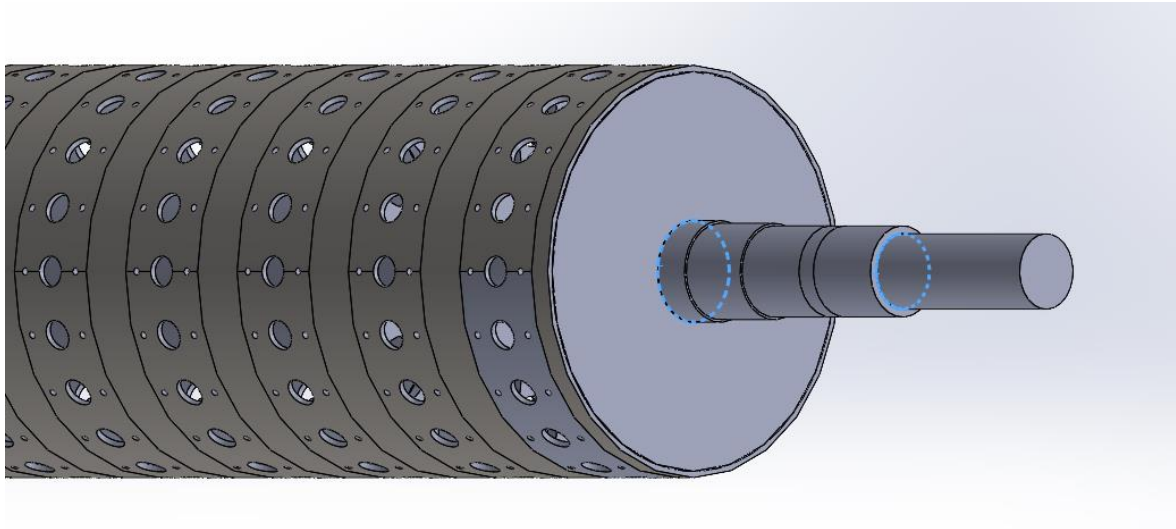


Figure 56. 2 critical point where fatigue stresses are defined on 26-disc-shaft.

6.2 Fatigue calculation

6.2.1 Mean stress.

The location on the drive end where the maximum stress is applied is called 1. The edge where the drive ends are attached to the vat at the support plate is called 2. The Von mise mean stress at those locations are defined by Simulation SolidWorks which is shown in the Figure 57.

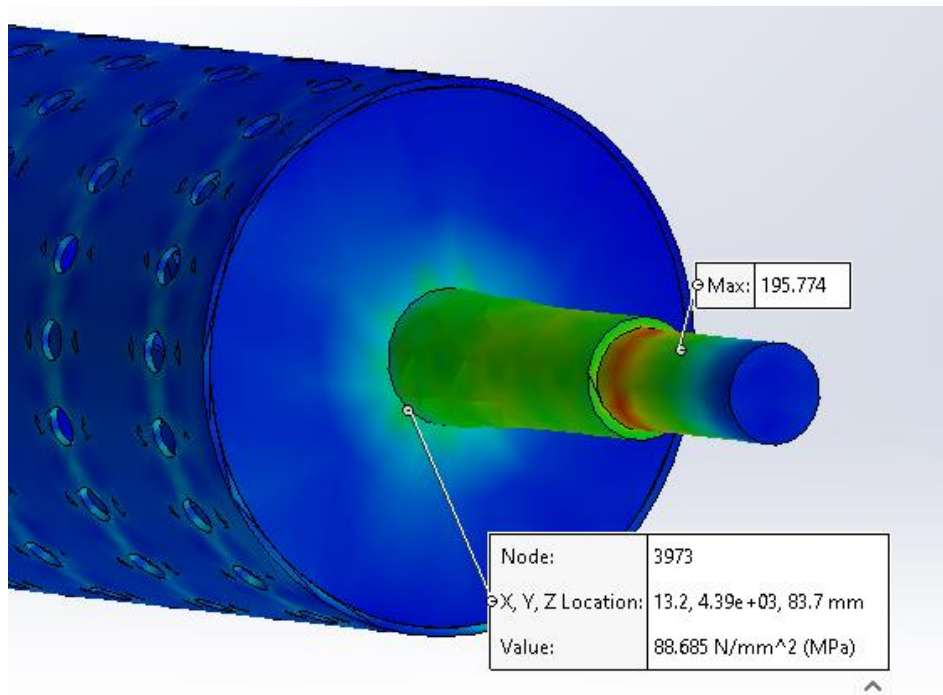


Figure 57. The mean stress of 2 critical points in 26-disc-shaft.

6.2.2 Amplitude stress

The torque, which is generated by the gear motor, is constant in theory. However, there is vibration or noise occurring by the motor during the operation, especially, when the motor is old and corrosive. In this calculation, the amplitude of torque is neglected because it affects trivially, compared to the one caused by the gearmotor. Because the shaft is rotating, the bending stress caused by the masses of the discs, inner channels, and gearmotor is

equal to the amplitude stress. The values of bending stresses which are the amplitude stress are shown in the Figure 58.

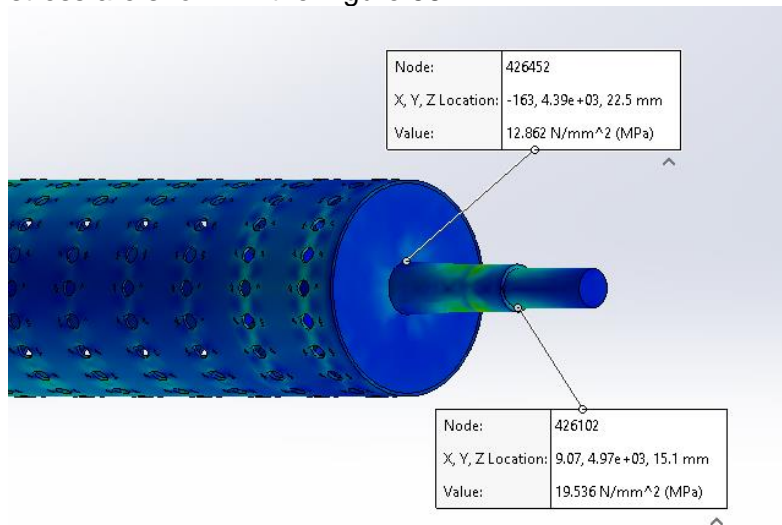


Figure 58. The amplitude stress at 2 critical stress in 26-disc-shaft.

6.2.3 Notch factor

The notch factor is included in the result by SolidWorks Simulation. Therefore, it is unnecessary to define the elastic notch factor in the calculation.

6.2.4 Reduction factor

- Size reduction factor

There are 2 sizes of the shaft which are 149 and 200 mm. According to Dowling, the reducing size factor of the first point which is 149 mm is equal to 0.7, which is shown in the Table 1. However, the size factor of other point is calculated by the formula of Niemann and Winter which is formula (42)

Depend on the material type, d_{Ref} and a_d are defined. The material of the shaft is stainless steel EN 1.4404, but it is assumed that the material of the shaft is the calculation is non-alloyed construction steel in order to define the coefficients. Therefore, the values of d_{Ref} and a_d are 40 mm and 0.15. respectively.

- Surface finish effects

The surface finish effect is defined by Brinell Hardness graph which is shown in the Figure 59. The ultimate strength of the material is 600 MPa which equals approximately 87 ksi. Moreover, the shaft is machined, hence, the surface finish effect is around 0.77 depending on the graph.

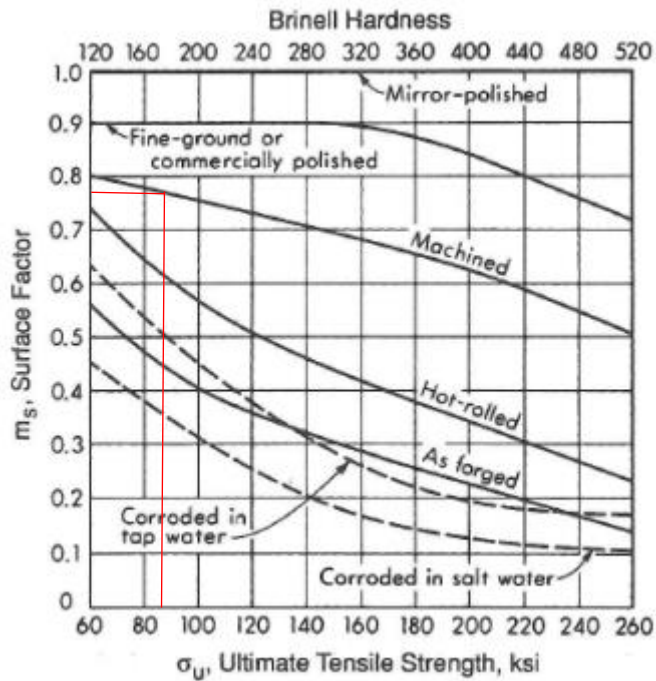


Figure 59. The Brinell Hardness graph.

- Other reduction

It is necessary to include two factors, which are corrosion and temperature effect in the calculation. It is assumed the material of the shaft is non-alloy construction steel during the calculation which corrodes during the operation. However, stainless steel is applied in practice which can be neglected the corrosive affection. During the operation, the operating temperature is in the range of 40 to 50 degrees Celsius, and the Thermo pulp is about 90 degrees. Hence, the factor is almost 1. In assumption, the other factor is equal to 1.

6.2.5 Fatigue calculation

The initial values of the 2 critical points and the material and factor properties are shown in Figure 60. The calculation of reducing factors is shown in Figure 61. The stresses and fatigue safety factor calculation is shown in Figure 62.

Shaft diameter	
$d_2 := 200 \text{ mm}$	$d_1 := 149 \text{ mm}$
Amplitude stress	
$\sigma_{a1} := 19.5 \text{ MPa}$	$\sigma_{a2} := 12.8 \text{ MPa}$
Mean stress	
$\sigma_{v1} := 195.7 \text{ MPa}$	$\sigma_{v2} := 88.69 \text{ MPa}$
Ultimate strength	
$Ru := 600 \text{ MPa}$	+

Figure 60. The initial value in fatigue calculation

Size reduction factor:	
$a_d := 0.15$	$d_{ref} := 40 \text{ mm}$
$m_{d1} := 0.7$	
$m_{d2} := \frac{1 - 0.7686 \cdot a_d \cdot \log\left(\frac{d_2}{7.5 \text{ mm}}\right)}{1 - 0.7686 \cdot a_d \cdot \log\left(\frac{d_{ref}}{7.5 \text{ mm}}\right)} = 0.912$	
Surface finish factor	
$Ru = 87.023 \text{ ksi}$	
$m_s := 0.77$	
Other factor	
$m_0 := 1$	
Overall reducing factor	
$m_1 := m_s \cdot m_0 \cdot m_{d1} = 0.539$	
$m_2 := m_s \cdot m_0 \cdot m_{d2} = 0.702$	

Figure 61. The reducing factors in fatigue calculation.

Fatigue limit

$$\sigma_{e1} := \frac{1}{2} \cdot (Ru - \sigma_{v1}) = (2.022 \cdot 10^8) \text{ Pa}$$

$$\sigma_{e2} := \frac{1}{2} \cdot (Ru - \sigma_{v2}) = (2.557 \cdot 10^8) \text{ Pa}$$

Modified fatigue limit (including reducing factor)

$$\sigma_{eF1} := m_1 \cdot \sigma_{e1} = (1.09 \cdot 10^8) \text{ Pa}$$

$$\sigma_{eF2} := m_2 \cdot \sigma_{e2} = (1.795 \cdot 10^8) \text{ Pa}$$

Dynamic safety factor

$$s_1 := \frac{\sigma_{e1}}{\sigma_{a1}} = 10.367$$

$$s_2 := \frac{\sigma_{e2}}{\sigma_{a2}} = 19.973$$

Figure 62. The calculation of stress and safety factor

6.3 Conclusion

It can be seen from the result that the safety factors of both critical points are favorable, which are 10.3 and 19.9, respectively. It is ensured that there is not any failure during the operation.

7 Developing the structure of the shaft

7.1 Introduction

After the strength analysis including static and fatigue, the structure development is made. There are 2 main goals of the development which are optimizing the material usage and increasing the inside cross-area of the inner channel. Several solutions are generated and tested; however, the milestone and final solutions are reported. The strength analyses of the updated structure are run by SolidWorks Simulation. In optimizing the material of the shaft, there are 2 solutions that are decreasing the thickness of the shaft and the length of the drive end. Besides increasing the cross-section of the inner channel, the cost and manufacturing process are considered.

7.2 Optimizing the usage of material.

7.2.1 Decreasing the length of the drive end

It is clear from the previous analyses that the torque is the most significant load effects on the drive end. The location of the support plate does not affect the drive end meaningfully. Hence, the distance between 2 support plates at the beginning of the shaft is decreased from 550 to 300 mm, which leads to the reduction in the length of the shaft. The part that connects the 2 support plates of the drive end is reduced by 250 mm which is shown in Figure 63. The stress plot of the shortened drive end model is shown in the Figure 64 by Simulation and the model is strong enough to carry the loads and the maximum Von mise stress is located on the beginning support plate which is 211.55 MPa.

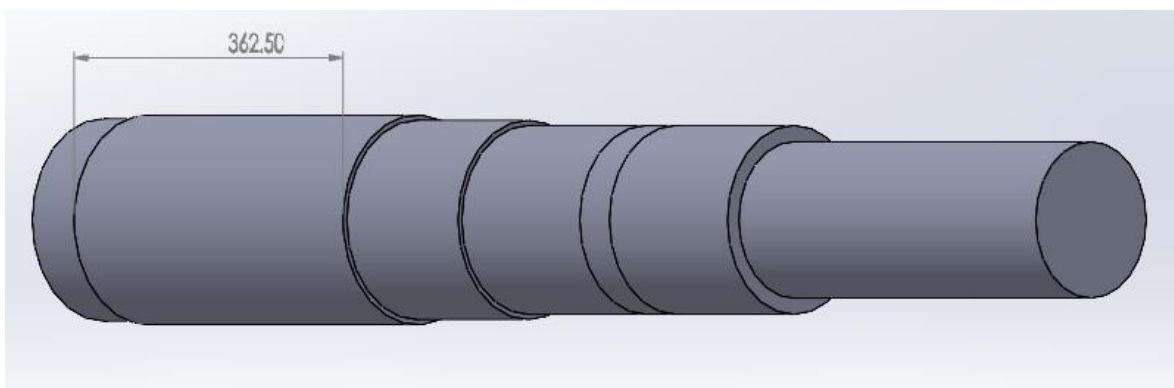


Figure 63. The shortened drive end.

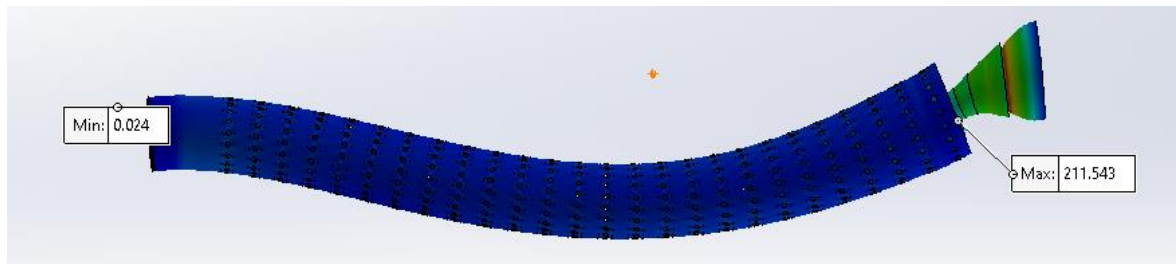


Figure 64. The stress plot of shorten drive end 26-disc-shaft.

7.2.2 Decreasing the thickness off the vat

In the latest model, the thickness of the vat is 12.5 mm. In the beginning, the thickness is decreased to 10 mm and the stress plot of the model is shown in Figure 65. It can be seen from the plot that, the structure is able to take the loads, especially the support plates. After that, the thickness is reduced to the minimum allowable thickness which is 6 mm. The thickness can not be smaller than 6 mm to ensure the fastening. The stress plot of 6 mm thickness 26-discs-shaft is shown in Figure 66, the support plate is still able to carry the load.

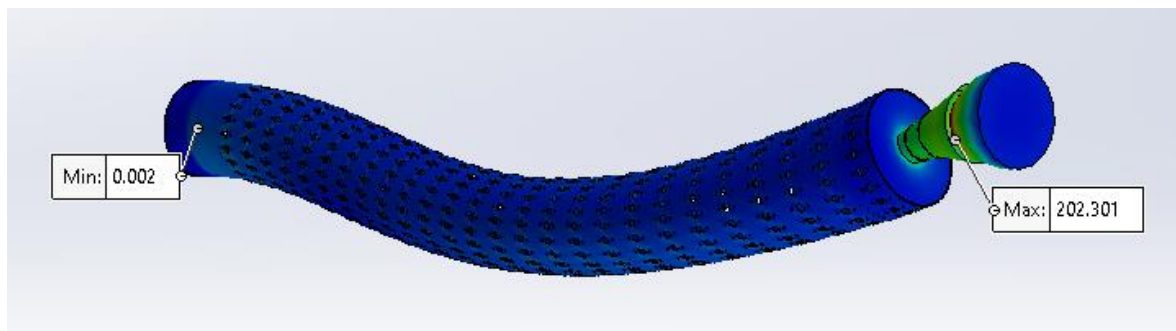


Figure 65. The stress plot of 10 mm thickness 26-disc-shaft.

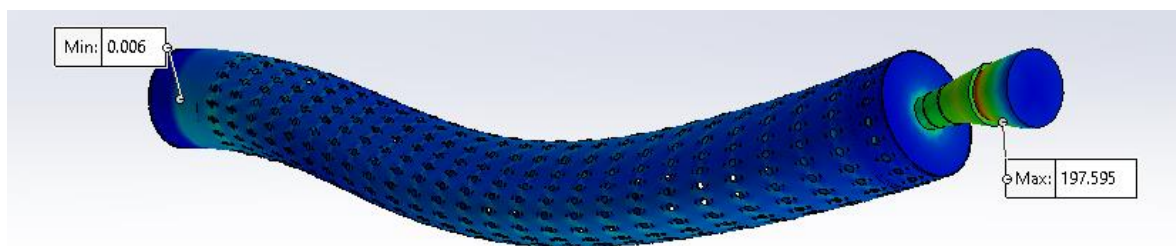


Figure 66. The stress plot of 6 mm thickness 26-disc-shaft.

7.3 Increasing the cross area of the inner channel

7.3.1 Introduction

In the latest model, the cross area of the channel is circle and the much of space inside the vat is wasted. Increasing the area of the channels leads to the improvement of the water flow. The less the thickness is, the more space inside the vat is, which the channels are

expanded. Hence, the channel is designed for 6 mm thickness 26-disc-shaft. Moreover, the support plate is updated, and the strength analysis of the updated shaft is run by Solid-Works.

7.3.2 Support plate

In the Figure 67 of Appendix 2, the latest model of the support plate, in which the cross area of the channel is circle, is shown. The area of the channels is increased as much as possible, therefore, they attached directly to the vat and the drive end. The updated profile of the support plate, which attached to the drive end, and the one at the end of the shaft are shown in the Figure 68 and 69 of Appendix 2, respectively. For the one attached to the drive end, it is assembled by 20 L-bar which is shown in the Figure 70 of Appendix 2 since the ease of manufacturing.

7.4 Inner channel

Depend on the area on the support plate, the profile of the channel is shown in the Figure 71 of Appendix 2. The thickness of the channel is minimized to increase the cross area which is 1 mm. The stress plot of the inner channels is simulated by SolidWorks and showed in the Figure 73. The channel carries the pressure inside by the vacuum which the magnitude is 0.4 bar. The fixtures are the face that the channel attached to the support plates, the vat, and the drive end which are showed in the Figure 72 of Appendix 2. The area of the updated channel is 21027.657 square millimetres.

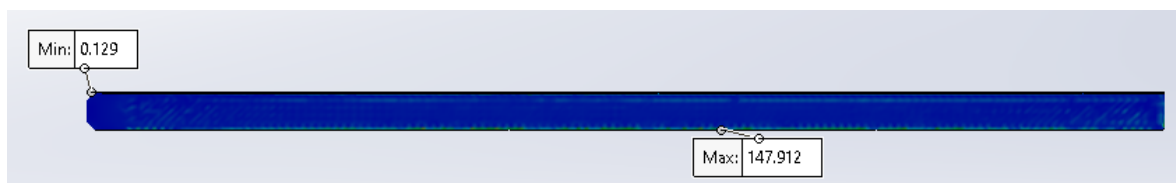


Figure 73. The stress plot of inner channel.

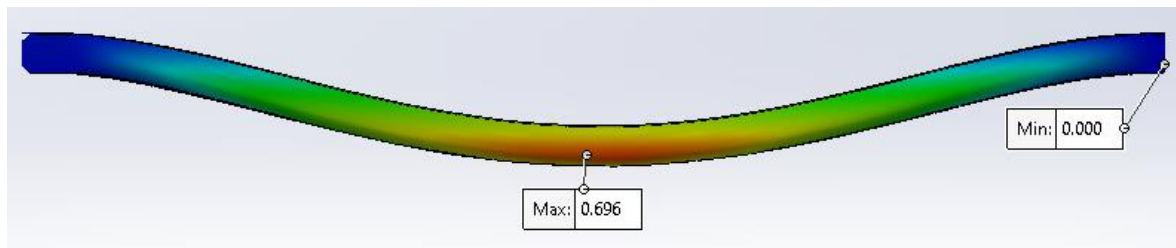


Figure 74. Displacement plot of inner channel.

7.4.1 Strength analyzation of the updated shaft

The strength analysis of the updated shafted including the updated inner channels and support plates is run by SolidWorks. The fixtures and external force are remained except the

forces by the channels on the support plates. The mass of the channels is replaced by the remoted load which the property is showed in the Figure 75, in order to give the accurate result for the final model. The stress and displacement result of the updated model are showed in the Figure 77 and 78. It is can be seen from the plots that there are not any failure or collision during the operation.

```

Mass = 103483.59 grams

Volume = 12935448.51 cubic millimeters

Surface area = 12938493.37 square millimeters

Center of mass: ( millimeters )
X = 0.00
Y = 266.40
Z = 4357.50

Principal axes of inertia and principal moments of inertia: ( grams * square millimeters )
Taken at the center of mass.
Ix = ( 0.00, 0.00, 1.00)    Px = 1163407591.37
Iy = ( 0.00, -1.00, 0.00)  Py = 655120721741.67
Iz = ( 1.00, 0.00, 0.00)   Pz = 655993566240.19

Moments of inertia: ( grams * square millimeters )
Taken at the center of mass and aligned with the output coordinate system.
Lxx = 655993566240.25    Lxy = 0.00    Lxz = 0.00
Lyx = 0.00              Lyy = 655120721741.61    Lyz = 0.00
Lzx = 0.00              Lzy = 0.00    Lzz = 1163407591.37

```

Figure 75. The mass property of the inner channel.

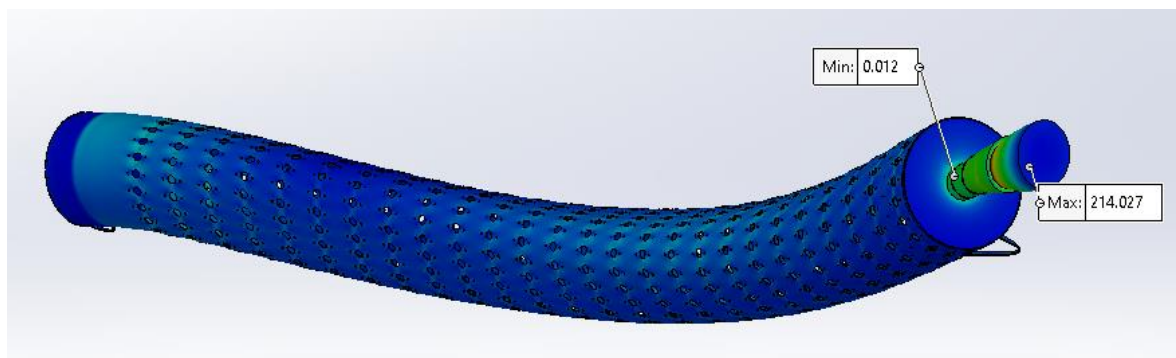


Figure 77. The stress plot of updated 26-disc-shaft

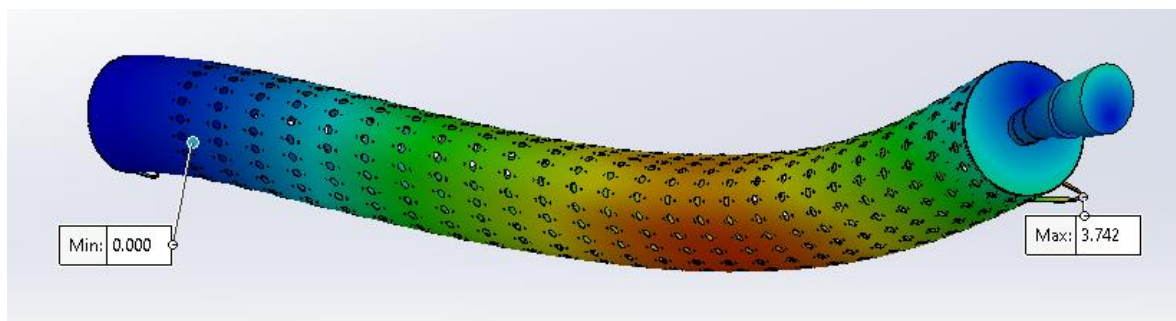


Figure 78. The displacement plot of updated 26-disc-shaft

7.5 Conclusion

The volume of the material in the updated shaft, which do not include the inner channels, is 169999424.18 cubic millimetre which decreased by approximately 46%. Moreover, the inside area of the updated inner channel is 21027.657 square millimetre which increased by roundly 71%. However, the more inside area of the channel is, the more material is used. The updates channel volume is 12935448.51 cubic millimetre which increased by about 89%. Overall, the volume of entire updated shaft is 428708394.38 cubic millimetre which grew by 35%.

8 Conclusion

After the analysis, it can be concluded that there is not any failure in structure and collision between the components during the operation of the latest Protcorb' s disc filter model. The static and the minimum fatigue safety factors of 26-disc-shaft are 2.7 and 10.2, respectively.

After the structure developing, the volume of the shaft without the channels decreased by 46%. The inside area of the updated channel increased by 71%, however, the material usage of the channel raised by 89%. Overall, the entire volume of updated shaft is 428708394.38 cubic millimeter which increased 35%.

In my opinion, the result of the thesis, which increases the filtration efficiency by 71%, is satisfactory. However, it leads to the increasing of the material and the manufacturing cost, which is caused by the welding process, of the plates. In the future, depend on the required filtration efficiency of the customer, the area of the inner channels is sizable. In case the needed area of the channels is smaller than the biggest one which is the result of the thesis, the manufacturing of the current plate (Figure 67) is applied. The cutting process is applied on a round plate which reduces the manufacturing cost. In addition, the area of inertia is increased, then the thickness of the plate can be cut down.

The thesis took a significant effort to complete. The combination of the approaches including 3D modelling, static and fatigue analyzing, is applied. Moreover, the new technics, which are the theorem of three moments and features in SolidWorks Simulation, and the deeply theoretical background of the applied methods are researched. After the thesis, I gain more experience and knowledge in strength analysis.

9 References

Dowling, N.E. 1999. Mechanical behaviour of materials. 2nd Edition. New Jersey: Prentice Hall.

Hibbeler, Russell C. 2018. Statics and Mechanics of Materials in SI Units. 3th Edition. Singapore: Prentice Hall.

Onouye, Barry S; Kane, Kevin. 2013. Statics and Strength of Materials for Architecture and Building Construction. 4th Edition. New York: Prentice Hall.

Kane, David S. 1987. Finite Element Analysis from concept to application. New Jersey: Addison-Wesley Publishing company.

Hibbeler Russell C. 2004. Engineering mechanics Statics. 3th Edition. Singapore: Prentice Hall.

eGyanKosh. 2017. Theorem of three moment. Retrieved on 03, February 2021. Available at <http://www.egyankosh.ac.in/bitstream/123456789/29506/1/Unit-6.pdf>.

SEW EURODRIVE. 2003. Industrial Gear Unit-M...Series. Retrieved on 03, February 2021. Available at <https://download.sew-eurodrive.com/download/pdf/11214805.pdf>.

HUBER SE. 2017. HUBER Disc Filter RoDisc-animation. Retrieved on 03, February 2021. Available at <https://www.youtube.com/watch?v=eINTh0u3KZk>.

Zero Gravity Filters. Water and process Fluid Filtration in the Pulp and Paper Industry. Retrieved on 03, February 2021. Available at <https://www.zgfilters.com/pulp-and-paper>.

Riker, Walter J. 1969. Continuous rotary disc filter. Patent. United States Patent Office. Retrieved on 03, February 2021. Available at <https://patentimages.storage.googleapis.com/f8/23/06/7e6ef4969ff06b/US3471026.pdf>.

Niemann, G; Winter, H. Winter; Höhn B.-R. 2005. Maschinenelemente Band 1: Konstruktion und Berechnung von Verbindungen, Lagern, Wellen. 4th Edition. Berlin: Springer-Verlag.

Appendix 1: The latest inner channel figures.

Appendix 2: The updated inner channel figures.